

1 **Sea-level variability and change along the Norwegian coast between 2003** 2 **and 2018 from satellite altimetry, tide gauges and hydrography**

3 Fabio Mangini¹, Léon Chafik^{2,3}, Antonio Bonaduce¹, Laurent Bertino¹, Jan Even Ø. Nilsen⁴

4 ¹Nansen Environmental and Remote Sensing Center and Bjerknes Centre for Climate Research, Bergen, Norway

5 ²Department of Meteorology and Bolin Centre for Climate Research, Stockholm, Sweden

6 ³National Oceanography Centre, Southampton, UK

7 ⁴Institute of Marine Research and Bjerknes Centre for Climate Research, Bergen, Norway

8 *Correspondence to:* Fabio Mangini (fabio.mangini@nersc.no)

9 **Abstract.** Sea-level variations in coastal areas can differ significantly from those in the nearby open ocean.
10 Monitoring coastal sea-level variations is therefore crucial to understand how climate variability can affect the
11 densely populated coastal regions of the globe. In this paper, we study the sea-level variability along the coast
12 of Norway by means of in situ records, satellite altimetry data, and a network of eight hydrographic stations
13 over a period spanning 16 years (from 2003 to 2018). At first, we evaluate the performance of the ALES-
14 reprocessed coastal altimetry dataset (1 Hz posting rate) by comparing it with the sea-level anomaly from tide
15 gauges over a range of timescales, which include the long-term trend, the annual cycle and the detrended and
16 deseasoned sea-level anomaly. We find that coastal altimetry and conventional altimetry products perform
17 similarly along the Norwegian coast. However, the agreement with tide-gauges in terms of trends is on average
18 6% better when we use the ALES coastal altimetry data. We later assess the steric contribution to the sea-level
19 along the Norwegian coast. While longer time series are necessary to evaluate the steric contribution to the
20 sea-level trends, we find that the sea-level annual cycle is more affected by variations in temperature than in
21 salinity, and that both temperature and salinity give a comparable contribution to the detrended and
22 deseasoned sea-level variability along the entire Norwegian coast. A conclusion from our study is that coastal
23 regions poorly covered by tide gauges can benefit from our satellite-based approach to study and monitor sea-
24 level change and variability.

25 **1 Introduction**

26 Global mean sea level (GMSL) has been rising during the XX century and the beginning of the XXI century at a
27 rate of approximately 1.5 mm yr^{-1} (Frederikse et al., 2020). Its rise is projected to continue, and even accelerate,
28 in the future (Hermans et al., 2021), thus posing significant stress on coastal communities (Nicholls, 2011). At a
29 local scale, though, sea-level variations can largely depart from the global average (Stammer et al., 2013).
30 Therefore, an accurate estimation and attribution of sea-level rise at regional scale is one of the major
31 challenges of climate research (Frederikse et al., 2018), with large societal benefit and impact due to the large
32 human population living in coastal areas (e.g., Lichter et al., 2011). The Norwegian coast is no exception. While
33 it appears little vulnerable to sea-level variations because of its steep topography and rocks resistant to erosion,
34 it has a large number of coastal cities, most of which have undergone significant urban development in recent
35 times (Simpson et al., 2015).

36

37 Since August 1992, when NASA and CNES launched the TOPEX/Poseidon mission, satellite altimetry has
38 enormously expanded our knowledge of the ocean and the climate system (e.g., Cazenave et al., 2018). With
39 the help of satellite altimetry, oceanographers and climate scientists could observe sea-level variations over
40 almost the entire ocean (e.g., Nerem et al., 2010; Madsen et al., 2019) and understand their causes (e.g.,
41 Richter et al., 2020), detect ocean currents (e.g., Zhang et al., 2007) and monitor their variability (e.g., Chafik et
42 al., 2015), observe the evolution of climate events (e.g., Ji et al., 2000) and investigate their origins (e.g., Picaut
43 et al., 2002). Satellite altimetry has made these, and other achievements, possible because it has provided
44 continuous sea-level observations over large parts of the ocean, in areas where sea-level measurements were
45 previously only occasional.

46

47 While invaluable over the open ocean, satellite altimetry measurements have historically been flagged as
48 unreliable in coastal areas (e.g., Benveniste et al., 2020). Indeed, the accuracy of radar altimetry, which is 2-3
49 cm over the open ocean (e.g., Volkov and Pujol, 2012), deteriorates in coastal regions because of technical
50 issues (e.g., Xu et al., 2019). Notably, large variations in the backscattering of the area illuminated by the radar
51 altimeters (for example, due to the presence of land or to patches of very calm water in sheltered areas;
52 Gómez-Enri et al., 2010) contaminate the returned echoes of radar altimeters, and the complex topography of

53 continental shelves, together with the irregular shape of most coastlines, makes geophysical corrections in
54 coastal areas less accurate than in the open ocean.

55

56 To increase the accuracy of radar altimetry in coastal regions, Passaro et al. (2014) have developed the Adaptive
57 Leading Edge Subwaveform (ALES) retracking algorithm. The ALES retracker addresses the altimeter footprint
58 contamination issue by avoiding echoes from bright targets (e.g., land). Several studies have found a clear
59 improvement of the ALES-reprocessed satellite altimetry observations over conventional altimetry products in
60 different areas of the World (e.g., Passaro et al., 2014, 2015, 2016, 2018, 2021), with the new algorithm
61 providing estimates of the altimetry parameters in coastal areas with levels of accuracy typical of the open
62 ocean for distances to the coast of up to 3 km circa (e.g., Passaro et al., 2014).

63

64 In this paper, we investigate how the ALES-reprocessed satellite altimetry dataset resolves sea-level along the
65 coast of Norway compared to all the tide-gauge records available over the 16-year period between 2003 and
66 2018. Indeed, to the best of our knowledge, previous validation studies have not considered the entire
67 Norwegian coast, but only parts of it: Passaro et al. (2015) focused on the transition zone between the North
68 Sea and the Baltic Sea, whereas Rose et al. (2019) focused on Honningsvåg, in northern Norway. The Norwegian
69 coast also appears particularly interesting for validation purposes because, during the altimetry period, it is well
70 covered by tide gauges, and because conventional altimetry products have previously failed to reproduce the
71 sea-level trends in the region (Breili et al., 2017). The present study will thus investigate the performance of
72 ALES in relation to these issues.

73

74 We further use the ALES-reprocessed altimetry dataset in combination with a network of hydrographic stations
75 along the coast of Norway to study the steric contribution to the sea-level variability in the region, which is
76 known to be challenging at the regional scale (e.g., Raj et al., 2020; Richter et al., 2012). Richter et al. (2012)
77 have already used tide gauges and hydrographic stations to assess the different contributions to the Norwegian
78 sea-level variability between 1960 and 2010. However, compared to their study, we use the coastal altimetry
79 dataset to reconstruct a monthly mean sea-level time series centred over each hydrographic station. This is an
80 advantage over Richter et al. (2012) since some of the Norwegian tide gauges are located in sheltered areas and
81 might not be representative of the variability captured by the nearest hydrographic station (which can be as far

82 as 100 km apart). Moreover, compared to Richter et al. (2012), we analyse the annual cycle of the sea-level
83 more in detail by describing how its properties change along the Norwegian coast. Furthermore, sea-level
84 measurements from satellite altimetry, unlike those from tide gauges, do not need to be corrected for vertical
85 land motion.

86

87 This paper is organized as follows. Section 2 describes the data used in the coastal sea-level signal analysis. An
88 analysis of sea-level components retrieved by each observational instrument is provided in Section 3. The
89 coastal sea level from tide gauges and satellite altimetry are compared in terms of temporal variability and
90 trends in Section 4. Section 5 focuses on the steric contribution to the sea-level estimates from altimetry, tide
91 gauges, and hydrographic data. Section 6 summarizes and concludes.

92

93 **2 Data**

94 **2.1 ALES-reprocessed multi-mission satellite altimetry**

95 To provide more accurate sea-level estimates in coastal regions, the ALES retracker operates in two stages. At
96 first, it fits the leading edge of the waveform to have a rough estimate of the significant wave height (SWH).
97 Then, depending on the SWH, the algorithm selects a portion of the waveform (known as subwaveform) and fits
98 it to estimate the range (the distance between the satellite and the sea surface), the SWH and the backscatter
99 coefficient.

100

101 The dataset is freely available at the Open Altimetry Database website of the Technische Universität München
102 (<https://openadb.dgfi.tum.de/en/>). The European Space Agency (ESA) also provides, through The Sea Level
103 Climate Change Initiative Programme, a coastal satellite altimetry dataset reprocessed with the ALES-retracker.
104 However, it only covers the northern latitudes up to 60°N and, therefore, only part of the region of interest in
105 this study (Benveniste et al., 2020).

106

107 The dataset includes observations from the following altimetry missions: Envisat (version 3), Jason-1, Jason-1
108 extended mission, Jason-1 geodetic mission, Jason-2, Jason-2 extended mission, Jason 3, SARAL, SARAL drifting

109 phase. These are provided at a 1 Hz posting rate (equivalent to an along-track resolution of circa 7 km) and
110 cover the period from June 2002 to April 2020, with the exception of one data gap between November 2010
111 (end of Envisat) and March 2013 (start of SARAL) to the north of 66° N. Data from different missions have been
112 cross-calibrated, so that there are no inter-mission biases.

113

114 Prior to distribution, several corrections have been applied to the satellite altimetry data. Among them, the
115 geophysical corrections are of particular interest for the purpose of this study. Indeed, to validate the ALES-
116 reprocessed altimetry against the Norwegian tide gauges, the same physical signal must be removed from both
117 datasets. The geophysical corrections applied to the ALES-reprocessed altimetry data include the tidal and the
118 dynamic atmospheric corrections (COSTA user manual,
119 http://epic.awi.de/43972/1/User_Manual_COSTA_v1_0.pdf). The correction for ocean and pole tides has been
120 performed using the EOT11a tidal model. The solid Earth related tides have also been subtracted from the
121 orbital altitude but, as it leaves the altimetry data in sync with the tide gauges (which are based on the solid
122 Earth), this correction has no further interest for this study. The dynamic atmospheric correction (DAC),
123 available at <https://www.aviso.altimetry.fr/index.php?id=1278>, removes both the wind and the pressure
124 contribution to the sea-level variability at timescales shorter than 20 days, and only the pressure contribution to
125 the sea-level variability at longer timescales. The high-frequency component of the DAC is computed using the
126 Mog2D-G High Resolution barotropic model (Carrère and Lyard, 2003), and it is removed because it would
127 otherwise alias the altimetry data. The low-frequency component accounts for the static response of the sea-
128 level to changes in pressure, a phenomenon also known as inverse barometer effect (IBE), and according to
129 which a 1 hPa increase/decrease in sea-level pressure corresponds to a 1 cm decrease/increase in sea-level. To
130 validate the ALES-reprocessed altimetry against the Norwegian tide gauges, the relevant physical signals at the
131 relevant time scales must be removed from the tide gauge data (Section 2.2).

132

133 The producers of ALES flag some of the data as unreliable. More precisely, they recommend excluding
134 observations that fall within a distance of 3 km from the coast and whose sea-level anomaly (SLA), SWH, and
135 standard deviation exceed 2.5 m, 11 m, and 0.2 m respectively. We have followed these recommendations with
136 one exception: we have lowered the threshold on the sea-level anomaly from 2.5 to 1.5 m because this choice

137 leads to a better agreement between the tide gauges and the ALES altimetry dataset between Måløy and
138 Rørvik, along the west coast of Norway (Fig. 1).

139

140 **2.2 Tide gauges**

141 The Norwegian Mapping Authority (Kartverket) provides information on observed water levels at 24 permanent
142 tide gauge stations along the coast of Norway. Data are updated, referenced to a common datum, quality
143 checked, and freely distributed through a dedicated web API (api.sehavniva.no).

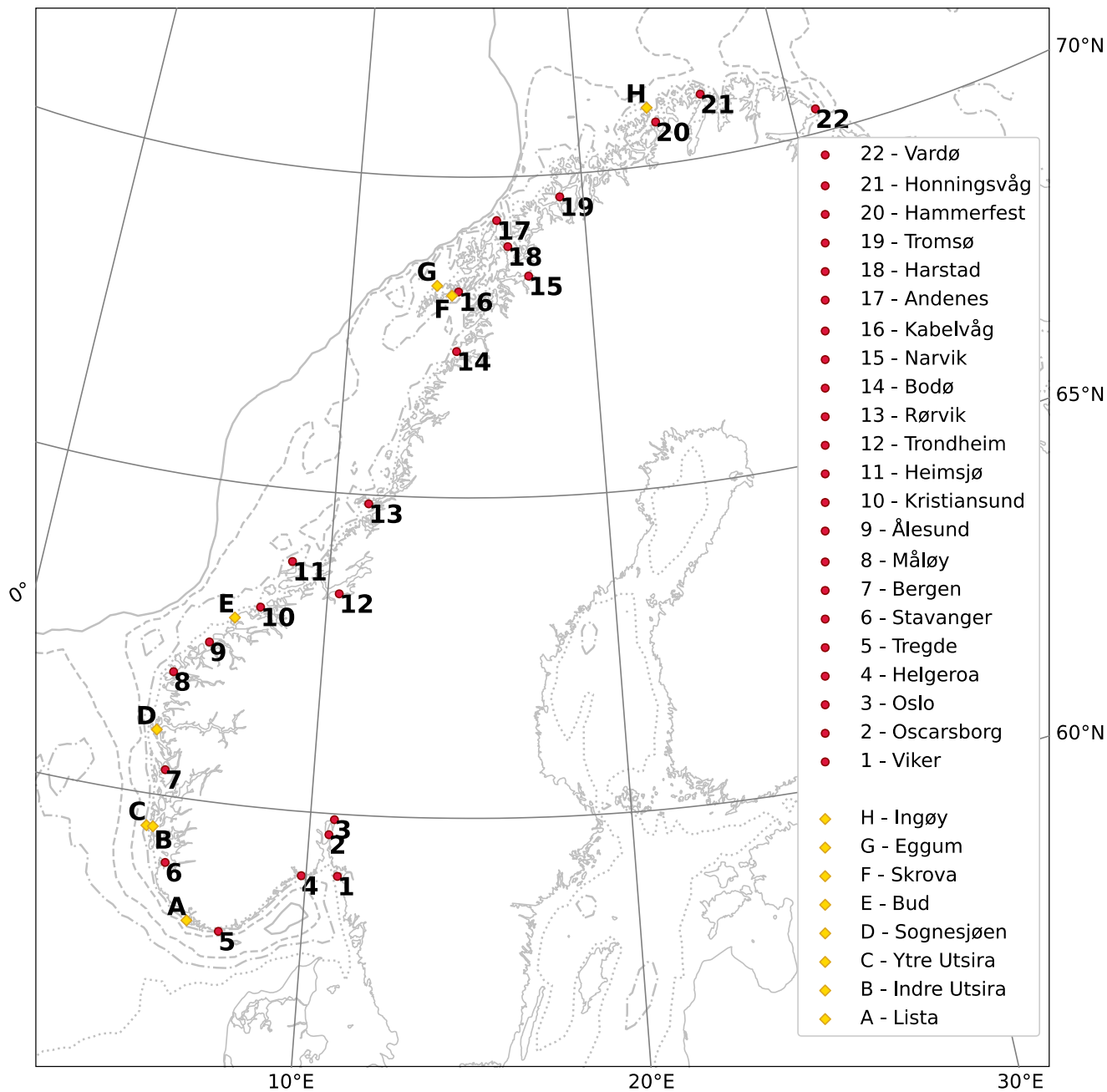
144

145 Even though most tide gauges provide a few decades of sea-level measurements, in this study we only consider
146 the period between January 2003 and December 2018 because it overlaps with the time-window spanned by
147 the ALES-altimetry dataset. Moreover, we only select 22 of the 24 permanent tide gauges available: we exclude
148 Mausund, since it has no measurements available before November 2010, and Ny-Ålesund, because it is outside
149 of our region of interest.

150

151 Over the period considered, the only tide gauges with missing values are Heimsjø and Hammerfest, with a 1-
152 month gap, and Oslo, with a 2-month gap. We expect the Norwegian set of tide gauges to map the coastal sea-
153 level with a spatial resolution of circa 130 km as it corresponds to the mean distance between adjacent tide
154 gauges. This estimate should be treated only as a first order approximation of the spatial resolution since the
155 distance between adjacent tide gauges varies along the Norwegian coast and ranges from ~30 km, in southern
156 Norway, to ~300 km, in western Norway (more precisely, between Rørvik and Bodø).

157



158
 159 Figure 1: Location of the tide gauges and of the hydrographic stations considered in this study (red circles and yellow diamonds
 160 respectively). The solid, dashed, dash-dotted and dotted light gray lines indicate the 500 m, 300 m, 150 m, and 50 m isobaths,
 161 respectively.

162

163 A number of geophysical corrections have been applied to the tide gauge data for them to be consistent with
164 the sea-level anomaly from altimetry. These include the effects of the glacial isostatic adjustment (GIA), the low
165 frequency tides, and the DAC.

166
167 The GIA results from the adjustment of the earth to the melting of the Fennoscandian ice sheet since the last
168 glacial maximum, circa 20 thousand years ago. The earth's relaxation affects substantially the sea-level change
169 relative to the Norwegian coast, with values ranging from approximately 1 up to 5 mm yr⁻¹ (e.g., Breili et al.,
170 2017). Along the Norwegian coast, the GIA affects the sea-level reading from the tide gauges because it induces
171 a vertical land movement (VLM) and, to a lesser extent the sea level itself, because it modifies the earth's
172 gravity field. The first effect has been corrected using both GNSS observations and levelling, whereas the second
173 has not been corrected since the satellite altimetry data are also influenced by geoid changes (Simpson et al.,
174 2017).

175
176 The low frequency constituents of ocean tide, derived from the EOT11a tidal model, are removed from the tide
177 gauge data as they are from the ALES-reprocessed altimetry dataset. Hammerfest, Honningsvåg and Vardø, the
178 three northernmost tide gauges (Fig. 1), are located outside of the EOT11a model domain. Therefore, at these
179 three locations, we remove the low frequency constituents of ocean tide for Tromsø. The constituents in
180 question are the solar semiannual, solar annual, and the nodal tide. For Norway the solar annual astronomical
181 tide is negligible, while the two latter constituents have amplitudes on the order of 1 cm. The nodal tide has a
182 period of approximately 18.61 years and results from the precession of the lunar nodes around the ecliptic
183 (Woodworth, 2012). As our time series are shorter than the nodal cycle, this constituent is not negligible with
184 regards to our trend analysis. None of the solid earth related tides needs to be removed from land-locked tide
185 gauge measurements to produce sea-level records comparable to altimetric sea surface height. Moreover, the
186 ocean pole tide, not provided by the EOT11a, has not been removed from the tide gauge data. However, it is
187 negligible in our region.

188
189 Since we have provided a description of the DAC in the previous section, here we only briefly describe how we
190 have applied it to the tide gauge data. At first, we have monthly averaged the six hourly DAC dataset (available
191 at the AVISO+ website, <https://www.avis0.altimetry.fr/en/data/products/auxiliary-products/dynamic->

192 [atmospheric-correction.html](#)). Then, for each tide gauge, we have computed the difference between the
193 monthly mean sea-level and DAC at the nearest grid point of the DAC product.

194

195 **2.3 Coastal hydrographic stations**

196 Over the time window covered by this study, the Institute of Marine Research (IMR) in Bergen, Norway, has
197 maintained eight permanent hydrographic stations over the Norwegian continental shelf, at a short distance
198 from the coast (Fig. 1). Data are updated and available at
199 <http://www.imr.no/forskning/forskningsdata/stasjoner/index.html>.

200

201 Along the Norwegian coast, the number of hydrographic stations is approximately one third the number of tide
202 gauges. Therefore, compared to the tide gauges, the hydrographic stations provide a coarser spatial resolution
203 of the physical properties of the ocean. We find that the distance between adjacent hydrographic stations is
204 approximately 250 km on average. This distance is minimum between the twin stations Indre Utsira/Ytre Utsira
205 and Eggum/Skrova, where it does not exceed 30 km, whereas it is maximum in western Norway, between Bud
206 and Skrova, where it is approximately 670 km.

207

208 We select the temperature and salinity profiles taken between January 2003 and December 2018 for them to
209 overlap with the period covered by the ALES-reprocessed altimetry dataset. The data are irregularly sampled,
210 being them mostly collected once every one or two weeks. To allow a comparison with the satellite altimetry
211 dataset, we have monthly averaged the temperature and salinity profiles at each hydrographic station. We
212 should note that the monthly-averaged time series of temperature and salinity contain missing values (Fig. 2).
213 Bud has the largest number of missing values, with 76 gaps out of 192. It is followed by Indre Utsira and Ytre
214 Utsira, with 44 and 41 gaps, respectively. The remaining hydrographic stations have less than 16 gaps each.

215

216 The hydrographic data were used to obtain estimates of the thermosteric and the halosteric sea-level
217 components over the spatial domain considered in this study.

218

219
220

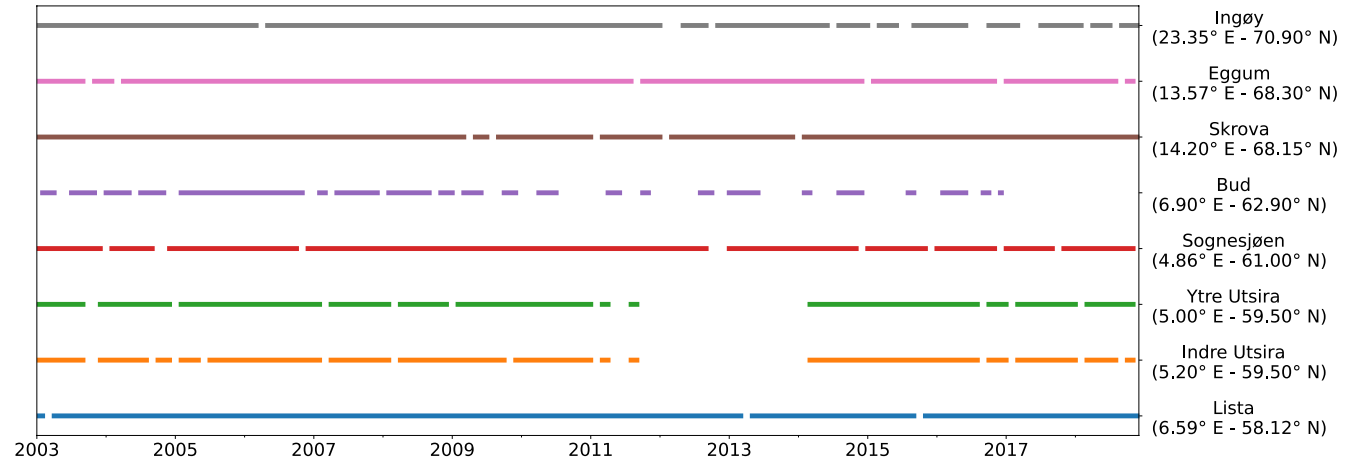


Figure 2: Data available at each hydrographic station between 01 January 2003 and 31 December 2018.

221

222 3 Methods

223 3.1 Harmonic analysis of sea-level

224 Following a similar approach to the one found in previous papers (e.g., Cipollini et al., 2017; Breili et al., 2017),
225 we use the Levenberg-Marquardt algorithm and fit the following function to sea-level records from remote
226 sensing and in situ data:

227

$$228 z(t) = a + b \cdot t + c \cdot \sin(2\pi t + d) + e \cdot \sin(4\pi t + f), \quad (1)$$

229

230 where a is the offset, b the linear trend, c and d the amplitude and the phase of the annual cycle, e and f the
231 amplitude and the phase of the semi-annual cycle. Then, we compare the linear trend, the amplitude and the
232 phase of the annual cycle, and the detrended, deseasoned sea-level signals from remote sensing and in situ
233 data. It is important to note that the use of this formula does not account for interannual variations of the
234 seasonal cycle.

235

236 In this study, we present the estimates of the sea-level trend from both satellite altimetry and the tide gauges
237 with the corresponding 95% confidence intervals (see below). Moreover, we assess how strongly the linear
238 trends from altimetry depend on the time period considered and show those trends that are significant at a

239 0.05 significance level (see below). To compute the confidence intervals and the statistical significance, we
240 account for the serial correlation in the time series. Indeed, successive values in the sea-level time series might
241 be significantly correlated and, therefore, not drawn from a random sample. To account for this non-zero
242 correlation, we compute the semi-variogram of the detrended and deseasoned SLA from satellite altimetry and
243 the tide gauges and then determine the effective number of degrees of freedom, N^* , for each time series
244 (Wackernagel, 2003), as described in Appendix A. To compute the 95% confidence interval of the linear trends,
245 we then use formula (7) in appendix A. Together with the semi-variogram, we also estimate the effective
246 number of degrees of freedom using the formula $N^* = N \cdot \frac{1-r_1}{1+r_1}$, where N is length of the time series and r_1 is its
247 lag-1 autocorrelation (Bartlett, 1935). However, in this paper, we opt for the more stringent approach and only
248 present the confidence interval derived using the semi-variograms. Indeed, we find that the semi-variogram
249 approach returns either the same or fewer effective number of degrees of freedom (not shown) when
250 compared to the other method. This is not the case for the effective number of the degrees of freedom of the
251 detrended and deseasoned SLA difference between ALES and the tide gauges. However, we find that the choice
252 of the approach does not alter our conclusions.

253

254 **3.2 Colocation of satellite altimetry and tide gauges**

255 To compare the sea-level from satellite altimetry and tide gauges, we first need to preprocess the altimetry
256 observations since these are not colocated neither in space nor in time with the tide gauges. The colocation
257 consists of two steps. At first, we select the altimetry observations that are located nearby each tide gauge.
258 Then, we average these observations both in space and in time to create, for each tide gauge location, a single
259 time series of monthly mean sea-level anomaly from altimetry.

260

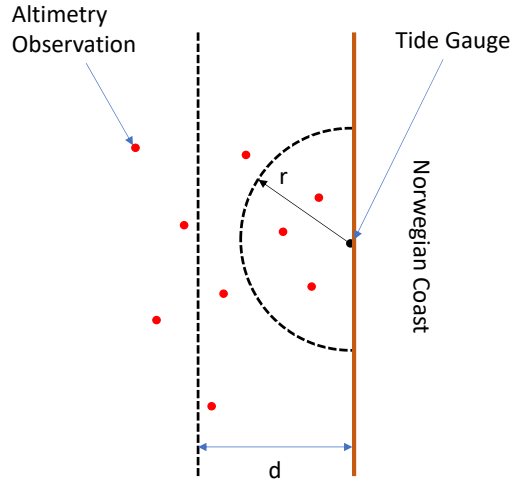
261 During the process, we verify that the selected altimetry observations represent the sea-level variability at each
262 tide gauge location. More precisely, since tide gauges represent the sea-level variability along a stretch of the
263 coast, we monthly average all the altimetry observations within a certain distance “d” from the coast and a
264 certain radius “r” from the tide gauge (Fig. 3). We try different combinations of d and r by allowing the first to
265 range between 5 and 20 km, with steps of 2.5 km, and the second between 20 and 200 km, with steps of 15 km.

266 Then, we pick the combination that maximizes the linear correlation coefficient between the detrended and
267 deseasoned SLA measured by satellite altimetry and by the tide gauge (as, for example, in Cipollini et al., 2017).
268 To set the maximum values of d and r at 20 and 200 km respectively, we have first performed a sensitivity test
269 and noted that larger values of d and r return slightly higher linear correlation coefficients (especially in
270 northern Norway), but do not alter the main results of this study. At the same time, a maximum distance of 20
271 km from the coast and of 200 km from the tide gauge ensures that all the selected altimetry points are located
272 over the continental shelf and that we can better capture the spatial scale variability of the seasonal cycle of the
273 sea level and of the sea-level trend.

274

275 We use the process described above to build a time series of monthly mean sea-level anomaly from altimetry at
276 each tide gauge location. The resulting sea-level time series have no missing values between Viker and Bodø.
277 Instead, to the north of Bodø, they have 29 missing values which result from the lack of altimetry observations
278 between November 2010 and March 2013.

279



280

281 **Figure 3: Sketch to illustrate the procedure used to build a monthly averaged SLA time series from the ALES-reprocessed satellite**
 282 **altimetry dataset at each tide gauge location. The parameter r is the distance from the tide gauge, whereas d is the distance from**
 283 **the coast.**

284 3.3 Colocation of satellite altimetry and hydrographic stations

285 We preprocess the altimetry observations to examine the steric contribution to the sea-level variability at each
 286 hydrographic station since the two datasets are not colocated neither in space nor in time. More precisely, we
 287 select all the altimetry observations located within 20 km from the Norwegian coast and within 200 km from
 288 each hydrographic station. Then, for each station, we monthly average the altimetry observations to build a
 289 sea-level anomaly time series from altimetry. The results in the previous subsection give confidence that the
 290 monthly mean sea-level computed over such a large area is representative of the sea-level variability at each
 291 hydrographic station.

292

293 **3.4 Monthly mean thermosteric, halosteric and steric sea-level components**

294 To compute the thermosteric and the halosteric components of the sea-level variability at each hydrographic
295 station, we first monthly average the temperature and salinity profiles. Then, at each hydrographic station, we
296 compute the monthly mean thermosteric and the halosteric components of the sea-level as in Richter et al.
297 (2012):

298

$$299 \eta_t = \int \alpha(T^*, S^*) \cdot (T - T_0) dz, \quad (2)$$

$$300 \eta_s = - \int \beta(T^*, S^*) \cdot (S - S_0) dz, \quad (3)$$

301

302 where α and β are the coefficients of thermal expansion and haline contraction, both computed at $T^* = (T +$
303 $T_0)/2$ and $S^* = (S + S_0)/2$. For each hydrographic station, T_0 and S_0 are reference values and represent time-
304 mean temperature and salinity averaged over the entire water column (Siegismund et al., 2007).

305

306 The steric component of the sea-level at each hydrographic station, η_{st} , is simply the sum of the corresponding
307 thermosteric and halosteric components of the sea level (Gill and Niller, 1973).

308

309 **3.5 Steric contribution to the Norwegian sea level**

310 At each hydrographic station, we assess the contribution of temperature and salinity to the linear trend and the
311 seasonal cycle of the SLA, and to the detrended and deseasoned SLA.

312

313 We do not use the harmonic analysis approach to estimate the sea linear trend and the seasonal cycle of the
314 SLA and of the thermosteric, halosteric and steric components of the sea-level at each hydrographic station.
315 Instead, we use simple linear regression to estimate the linear trend and we compute the monthly climatology
316 of each detrended time series to estimate the corresponding seasonal cycle. Indeed, the seasonal cycle of the
317 SLA and of the thermosteric, halosteric and steric sea level might depart from the linear combination of the
318 annual and the semi-annual cycles.

319

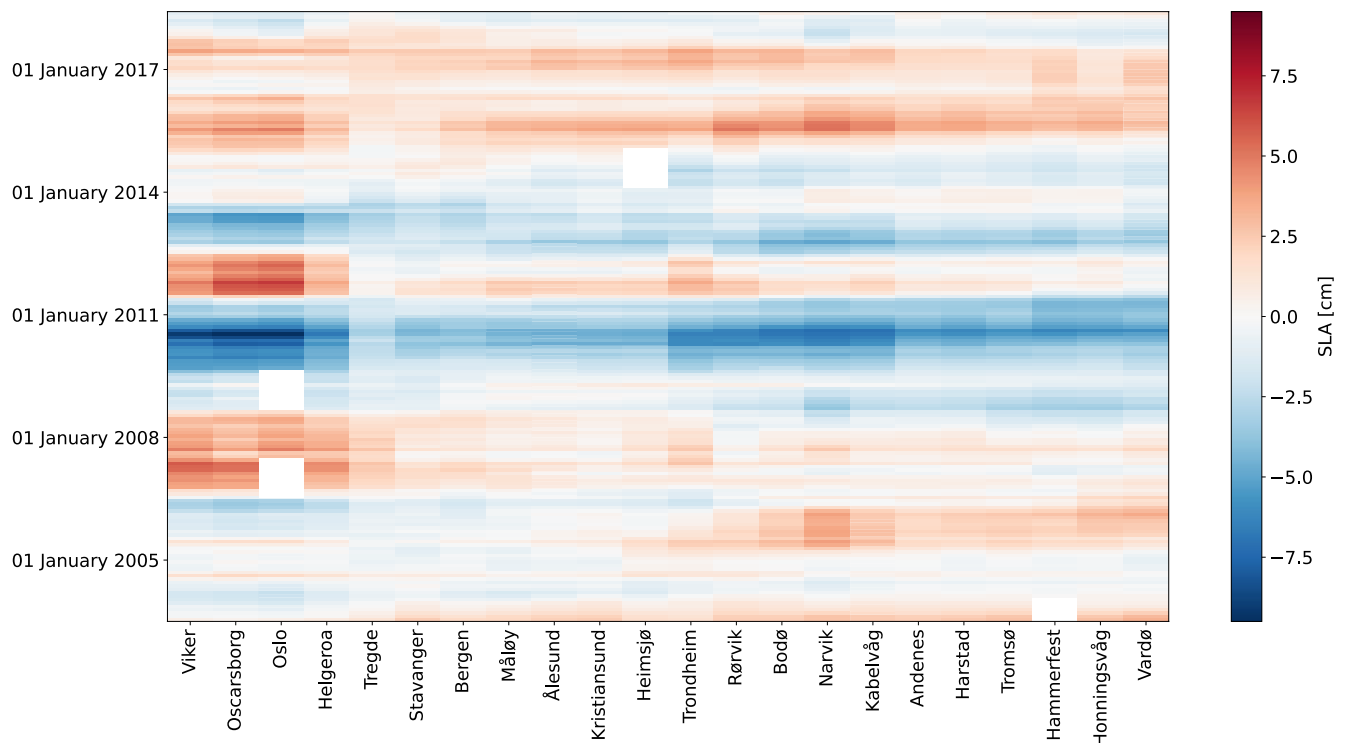
320 4 Comparison of satellite altimetry and tide gauges measurements

321 In this Section, we assess the quality of the ALES reprocessed coastal altimetry dataset against tide-gauge
322 records by comparing the detrended and deseasoned sea-level variability, the sea-level annual cycle and sea-
323 level trends provided by the remote-sensing and in situ data. We also focus on the stability of linear trend
324 estimates obtained from satellite altimetry (Liebmann et al., 2010; Bonaduce et al., 2016).

325

326 4.1 Detrended and deseasoned coastal sea-level

327



328

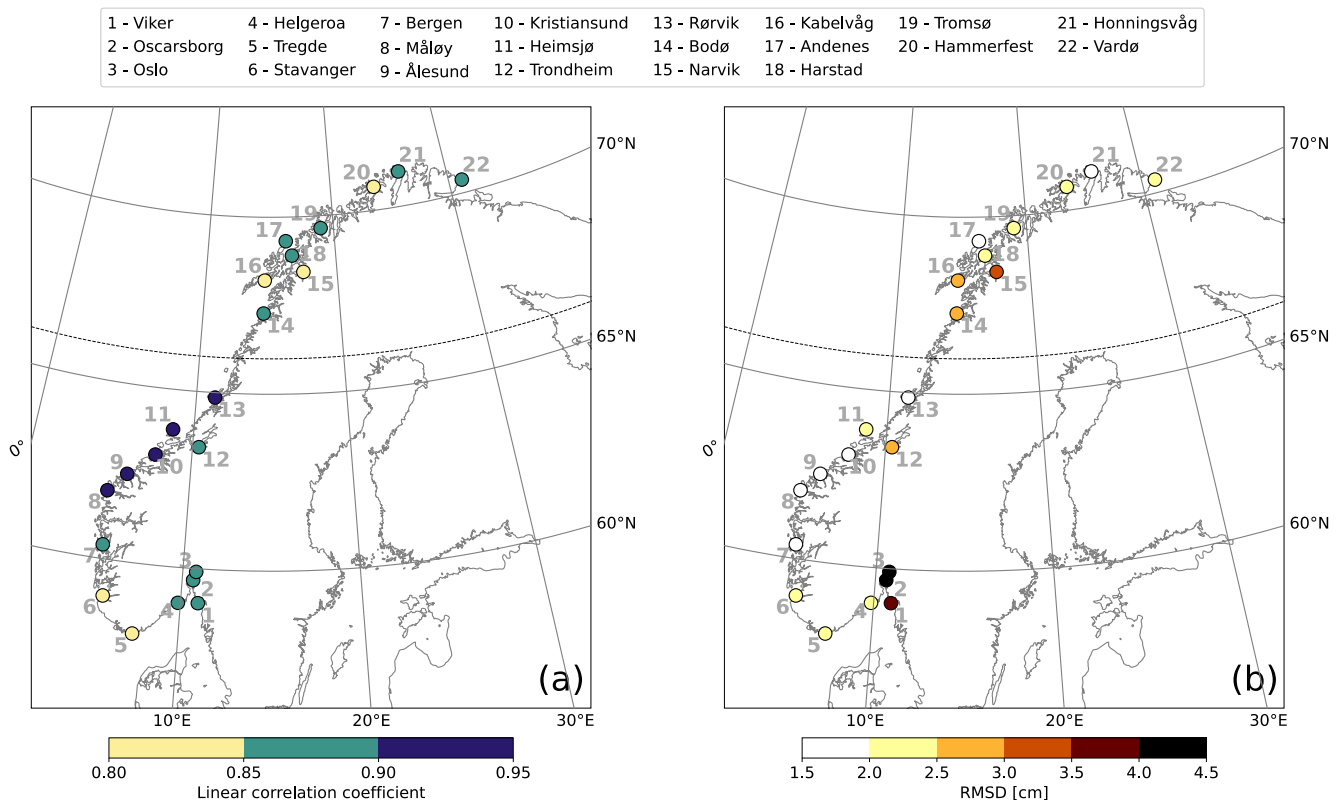
329 **Figure 4: Hovmöller diagram of the detrended and deseasoned monthly mean SLA from tide gauges. The SLA at each tide gauge has**
330 **been low-pass filtered with a one-year running mean. The tide gauges are displayed on the x-axis. Time is displayed on the y-axis and**
331 **increases from bottom to top.**

332

333

334 Before comparing the detrended and deseasoned SLA from altimetry and tide gauges, we briefly describe how
335 the detrended and deseasoned SLA evolves along the Norwegian coast during the period under study. More

336 precisely, we low-pass filter the detrended and deseasoned SLAs with a one-year running mean to identify their
 337 main features at each tide gauge location. Figure 4 shows years when the detrended and deseasoned SLA
 338 variations are coherent along the whole Norwegian coast, and years when the sea-level variability occurs at
 339 smaller spatial scales (between 100 and 1000 km). As an example, between mid-2009 and the beginning of 2011
 340 circa, the detrended and deseasoned SLA shows negative values of up to -6 cm along the entire Norwegian
 341 coast. On the contrary, between 2003 and mid-2009, we note a dipole pattern, with SLA with opposite sign in
 342 the south and in the north of Norway. Indeed, up to the beginning of 2006 circa, the Norwegian coast has
 343 experienced a negative SLA to the south of Hemsjø and a positive SLA to the north of Hemsjø. During the
 344 following three years, the opposite situation has occurred. These results suggest that, although coherent sea-
 345 level variability occurs along the Norwegian coast as seen from tide gauges, there are periods when it does not:
 346 during these periods, the sea-level variability is likely driven by local changes.
 347



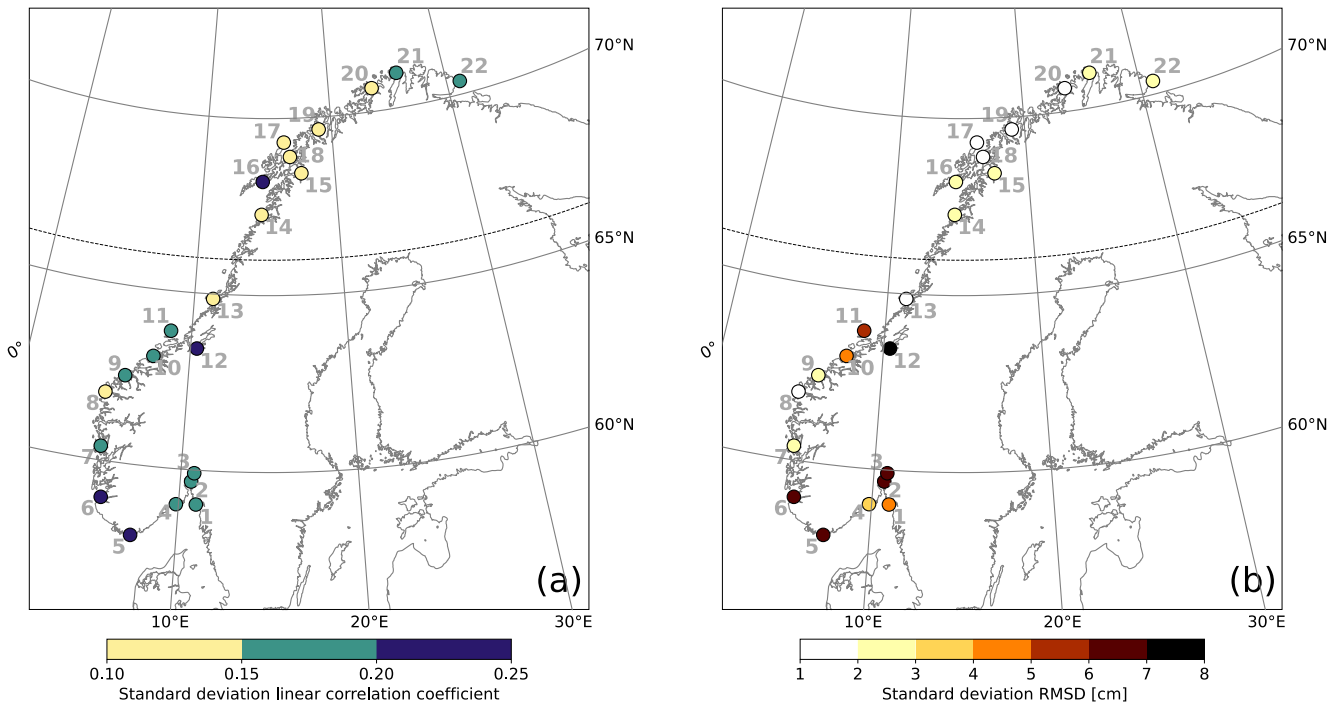
348
 349 **Figure 5: Comparison between coastal sea-level signals from in situ measurements and area-averaged remote-sensing data. At each**
 350 **tide gauge location, linear correlation coefficient (a) and RMSD (b) between the detrended and deseasoned monthly mean SLA from**
 351 **the ALES altimetry dataset and from the tide gauge. The black, dashed line indicates the 66° N parallel.**

352

353 Figure 5 shows a very good agreement between the detrended and deseasoned monthly mean SLA from ALES
354 and the tide gauges. The two datasets agree best along the west coast of Norway where, if we exclude
355 Trondheim, the linear correlation coefficients exceed 0.90 and the RMSDs range between 1.5 and 2.5 cm. As
356 expected, satellite altimetry performs better between Måløy and Rørvik than in southern and northern Norway
357 because of the convergence of altimeter tracks in the region. We suspect that Trondheim is an exception
358 because it is located in the Trondheim fjord, where satellite altimetry might not adequately capture local sea-
359 level variations: the presence of land and patches of calm water affects the quality of the satellite altimetry
360 measurements (Gómez-Enri et al., 2010; Abulaitijiang et al., 2015), and the complex bathymetry and coastline
361 hamper geophysical corrections (Cipollini et al., 2010). Similar peculiarities of the coastline along the Norwegian
362 Trench, in the Skagerrak and in the Oslo fjord, are also likely to affect the agreement, causing the linear
363 correlation coefficients to fall between 0.80 and 0.90 and the highest RMSDs to range between 2.5 and 4.5 cm.
364 Instead, in northern Norway, where we find linear correlation coefficients between 0.80 and 0.90 (statistically
365 significant at a 0.05 significance level) and RMSDs between 1.5 and 3 cm, the problem might result from the
366 smaller number of altimetry observations in the region. Indeed, only the tracks of Envisat, SARAL, SARAL drifting
367 phase cover the Norwegian coast north of 66° N.

368

1 - Vikør	4 - Helgeroa	7 - Bergen	10 - Kristiansund	13 - Rørvik	16 - Kabelvåg	19 - Tromsø	21 - Honningsvåg
2 - Oscarsborg	5 - Tregde	8 - Måløy	11 - Heimsjø	14 - Bodø	17 - Andenes	20 - Hammerfest	22 - Vardø
3 - Oslo	6 - Stavanger	9 - Ålesund	12 - Trondheim	15 - Narvik	18 - Harstad		



369
 370 **Figure 6: Comparison between coastal sea-level signals from in situ measurements and area-averaged remote-sensing data. At each**
 371 **tide gauge location, standard deviation of the linear correlation coefficients (a) and of the RMSDs (b) computed over each possible**
 372 **combination of the distance from the coast and of the distance from the tide gauge. The black, dashed line indicates the 66° N**
 373 **parallel.**
 374

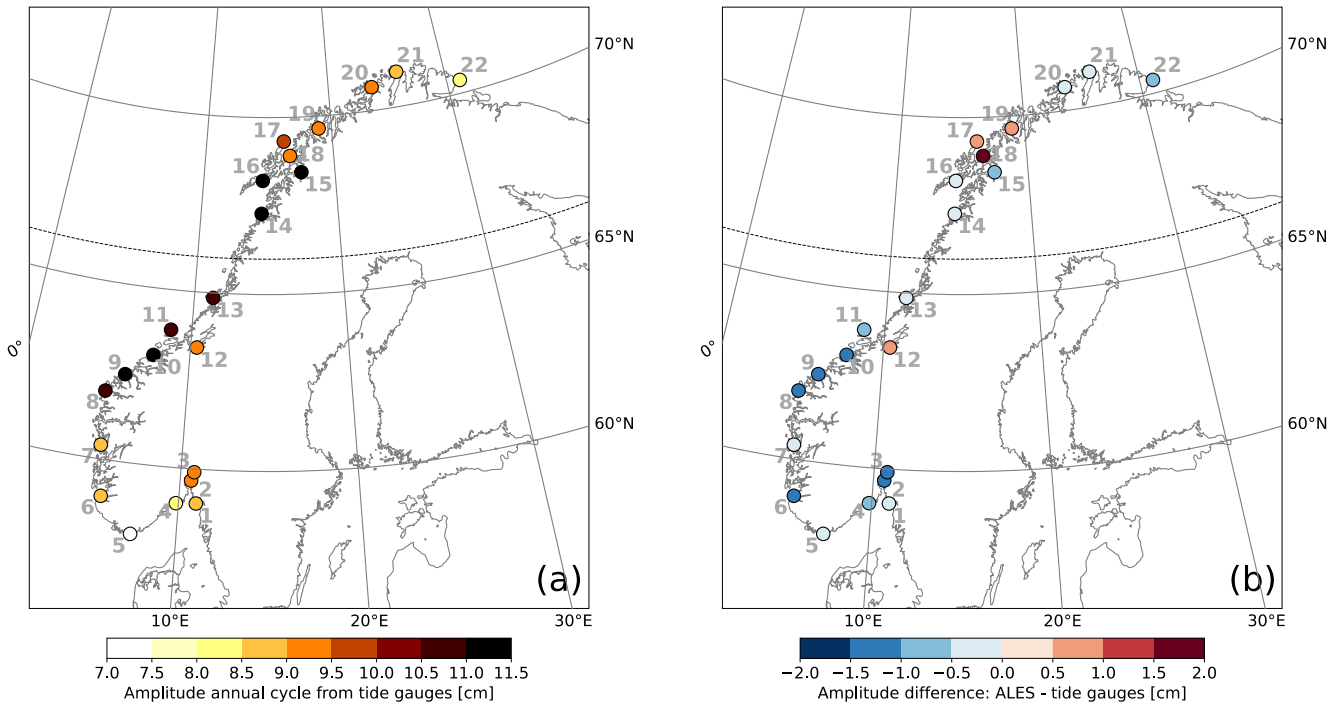
375 Figure 6 supports our previous conclusions on the relationship between satellite altimetry and the tide gauges
 376 at Trondheim, Oslo and Oscarsborg. In Figure 6, we show, for each tide gauge, the standard deviation of the
 377 linear correlation coefficient and of the RMSDs over all the possible combinations of the distance from the coast
 378 and from the tide gauge to measure the geometrical uncertainty of the SLA estimates from satellite altimetry.
 379 We find that, at Trondheim, both the linear correlation coefficient and the RMSD depend more on the size of
 380 the selection window when compared to other regions of the Norwegian coast. Similarly, at Oslo and
 381 Oscarsborg, we note an anomalously high standard deviation of the linear correlation coefficient. We expect
 382 anomalously high values of the standard deviation of the linear correlation coefficients and RMSDs because
 383 these three tide gauges are in sheltered areas (Trondheim in the Trondheim fjord, whereas Oslo and Oscarsborg

384 and the Oslofjord) which can favour the formation of patches of calm water and negatively affect the quality of
 385 the satellite altimetry observations.

386

387 **4.2 Annual cycle of coastal sea-level**

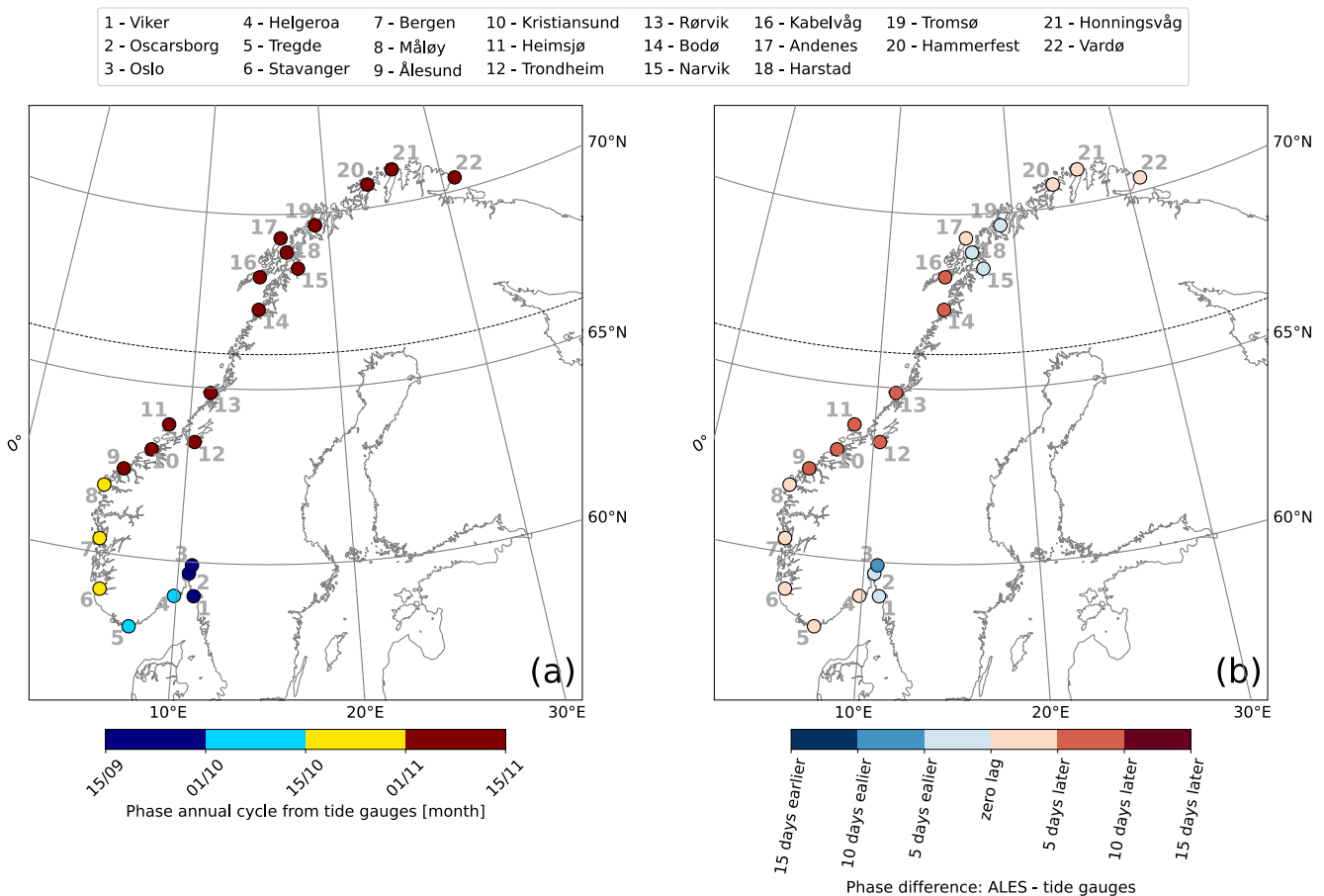
1 - Viker	4 - Helgeroa	7 - Bergen	10 - Kristiansund	13 - Rørvik	16 - Kabelvåg	19 - Tromsø	21 - Honningsvåg
2 - Oscarsborg	5 - Tregde	8 - Måløy	11 - Heimsjø	14 - Bodø	17 - Andenes	20 - Hammerfest	22 - Vardø
3 - Oslo	6 - Stavanger	9 - Ålesund	12 - Trondheim	15 - Narvik	18 - Harstad		



388
 389 **Figure 7: Comparison between the amplitude of coastal sea-level annual cycle from in situ measurements and area-averaged remote-**
 390 **sensing data. At each tide gauge location, amplitude of the annual cycle from the tide gauges (a) and difference between the**
 391 **amplitude of the annual cycle from the ALES-reprocessed altimetry dataset and the tide gauges (b). The black, dashed line indicates**
 392 **the 66° N parallel.**
 393

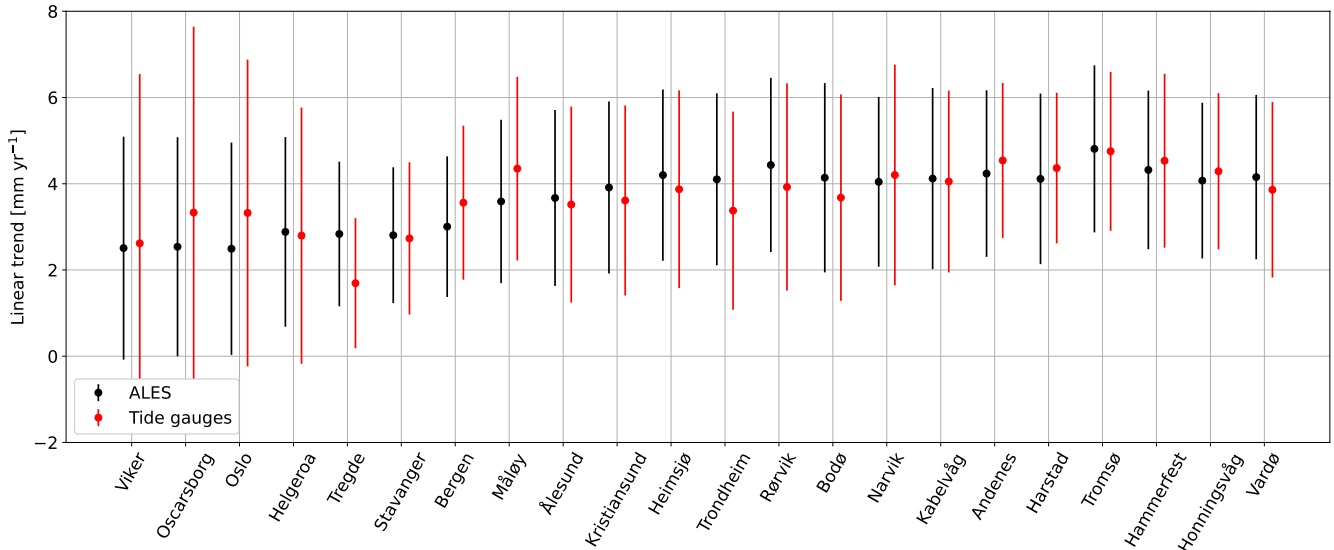
394 Figures 7 and 8 show a good agreement between the annual cycle estimated using the ALES altimetry dataset
 395 and the tide gauges. The difference between the amplitudes of the annual cycle from ALES and the tide gauges
 396 ranges between -1.2 and 1.8 cm. However, at most tide gauge locations (16 out of 22), the differences are much
 397 smaller, between -1 and 1 cm, less than 10 % of the amplitude of the corresponding annual cycle (Fig. 7a). We

398 note that the differences between the amplitudes are mostly negative along the southern and western coast of
 399 Norway and that, to the north of Rørвик, they become smaller, and even change sign at some locations (Fig. 7b).
 400
 401 The difference between the phases of the annual cycle estimated using the ALES altimetry dataset and the tide
 402 gauges ranges between -10 and +10 days (Fig. 8b). Such a great similarity indicates that both radar altimetry
 403 and the tide gauges capture the phase lag of approximately two months between the annual cycle in the north
 404 and in the south of Norway. The annual cycle peaks during the second half of September in the Skagerrak and in
 405 the Oslofjord region, in October along the Norwegian Trench and in south-west Norway, and mainly during the
 406 first week of November north of Kristiansund.
 407



408
 409 **Figure 8: Comparison between the phase of coastal sea-level annual cycle from in situ measurements and area-averaged remote-**
 410 **sensing data. At each tide gauge location, phase of the annual cycle from the tide gauges (a) and phase difference of the annual cycle**
 411 **from the ALES-reprocessed altimetry dataset and from the tide gauges (b). The black, dashed line indicates the 66° N parallel.**

412

413 **4.3 Linear trend of coastal sea-level**

414

415

416

417

Figure 9: At each tide gauge location, linear trend of the SLA from the ALES-reprocessed altimetry dataset (black dots) and from tide gauges (red dots). The error bars show the 95th confidence intervals of the sea-level trend at each tide gauge location.

418

419

420

421

422

423

424

425

426

427

428

429

430

The differences between sea-level trend estimates obtained from the in-situ and remote-sensed signals range between -0.85 and 1.15 mm yr^{-1} along the Norwegian coast (Fig. 9). Both datasets return a similar spatial dependence of the sea-level trend along the Norwegian coast, with the lowest values found in the Skagerrak and the Oslofjord (between 2 and 3 mm yr^{-1}), and the highest to the north of Heimsjø (around 4 mm yr^{-1}). Moreover, the two datasets return a similar uncertainty of the sea-level trend at each tide gauge location.

Despite their similarities, we still find that the difference between the sea-level trend from altimetry and tide gauges is significantly different from zero at a 0.05 significance level at 3 out of 22 tide gauges. Following Benveniste et al. (2020), we assess the significance in terms of fractional differences (*FDs*). Fractional differences are defined as $FD = |\tau| / (t_{0.05/2} \cdot SE \cdot \frac{N}{N^*})$, where $|\tau|$ is the absolute value of the linear trend of the SLA difference between altimetry and each tide gauge, $t_{0.05/2}$ is the critical value of the Student t-test distribution for a 95 % confidence level with $N^* - 2$ number of degrees of freedom, SE is the standard error, and N/N^* is the ratio between the total number of observations and the effective number of degrees of

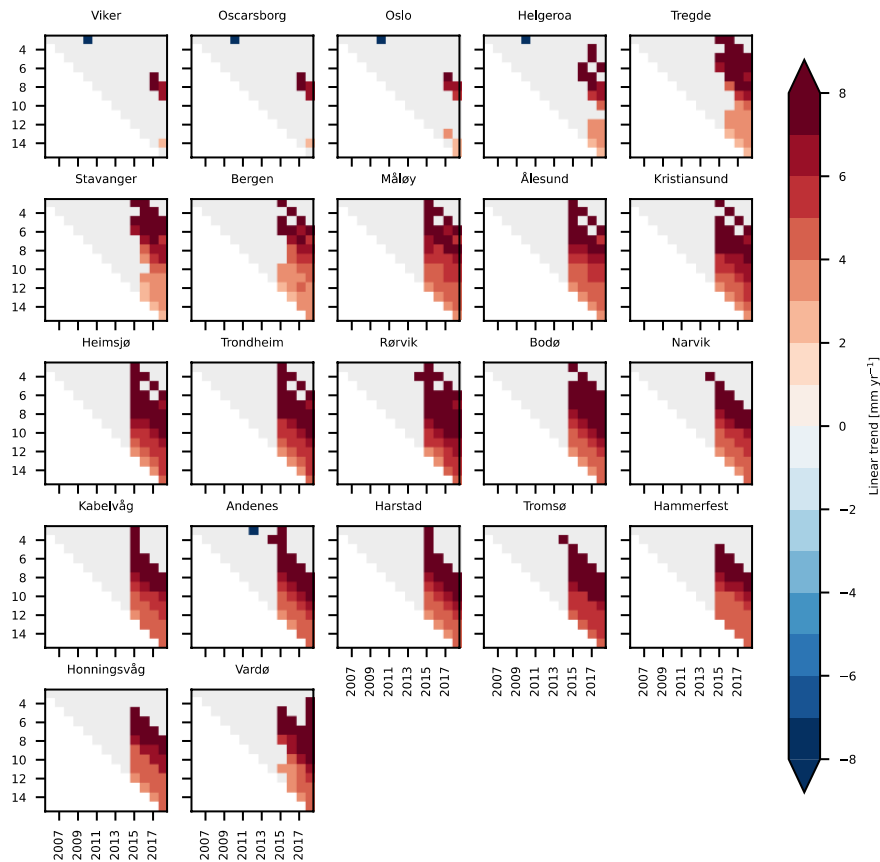
431 freedom. When $FD > 1$, the difference between the two trends is statistically significant at a 0.05 significance
432 level, a condition that occurs at Tregde, Måløy, and Bergen. Interestingly, none of these tide gauges is located
433 north of 66° N despite only some of the altimetry missions considered in this study have an inclination
434 exceeding 66° N (namely, Envisat, SARAL, SARAL drifting phase). Therefore, the fewer altimetry observations to
435 the north of 66° N seem not to deteriorate the agreement between the ALES-reprocessed altimetry and the tide
436 gauges.

437

438 Following Liebmann et al. (2010), we use the satellite altimetry data to assess how strongly the sea-level trend
439 depends on the time length of the period considered. Each point in Fig. 10 shows the sea-level trend computed
440 over the number of the years on the y-axis, up to the year specified on the x-axis. Between 2003 and 2013 circa,
441 we do not find a significant sea-level trend along the Norwegian coast. Indeed, with very few exceptions, the
442 trends are not statistically different from zero at a 0.05 significance level. The exceptions consist in a small
443 number of cases, each characterized by a sea-level trend lower than -4 mm yr^{-1} .

444

445 On the contrary, with the exception of three southernmost tide gauge locations, we note a significant positive
446 sea-level trend along the entire coast of Norway when the period considered for the calculation ends in 2015 or
447 later. The linear trends decrease as the length of the period selected increases. When sea-level rates are
448 computed over periods of a few years only, they even exceed 6 mm yr^{-1} . Instead, over longer periods of time
449 (e.g., more than 10 years), they mainly range between 3 and 5 mm yr^{-1} . A visual inspection of the time series
450 confirms that the sea-level has increased since 2014.



451
 452 **Figure 10: Stability of the sea-level trend along the Norwegian coast. At each tide gauge location, linear trend of the SLA from ALES as**
 453 **a function of the period considered. Each subplot refers to a tide gauge location and shows all the possible trends computed up to the**
 454 **year shown in the x-axis, considering the number of years displayed on the y-axis. For example, the point (x=2014, y=5) in each**
 455 **subplot shows the linear trend of the SLA computed over the 5 years period between 01 January 2009 and 31 December 2014. The**
 456 **light gray colour is used to mask those values that are not significantly different from zero at 0.05 significance level.**
 457

458

459 **5 Steric contribution to the sea-level variability**

460 In this Section, we use the Norwegian set of hydrographic stations to assess how temperature and salinity affect
 461 the sea-level trend, the seasonal cycle of sea-level and the detrended, deseasoned sea-level variability at
 462 different locations along the Norwegian coast.

463

464 **5.1 Variability of the thermosteric and the halosteric sea-level components**

465 The variability of the thermosteric and the halosteric sea-level components along the Norwegian coast mainly
466 occurs over two different spatial and temporal scales (Fig. 11). Notably, the seasonal cycle dominates the
467 thermosteric sea-level variability at each hydrographic station and is responsible for the thermosteric sea-level
468 to vary approximately uniformly along the coast of Norway. On the contrary, the halosteric component shows a
469 variability at shorter spatial- and temporal-scales, possibly due to the contributions from local rivers. The main
470 exceptions are, due to their proximity, the two sets of twin hydrographic stations, Indre Utsira-Ytre Utsira and
471 Eggum-Skrova (Fig. 1).

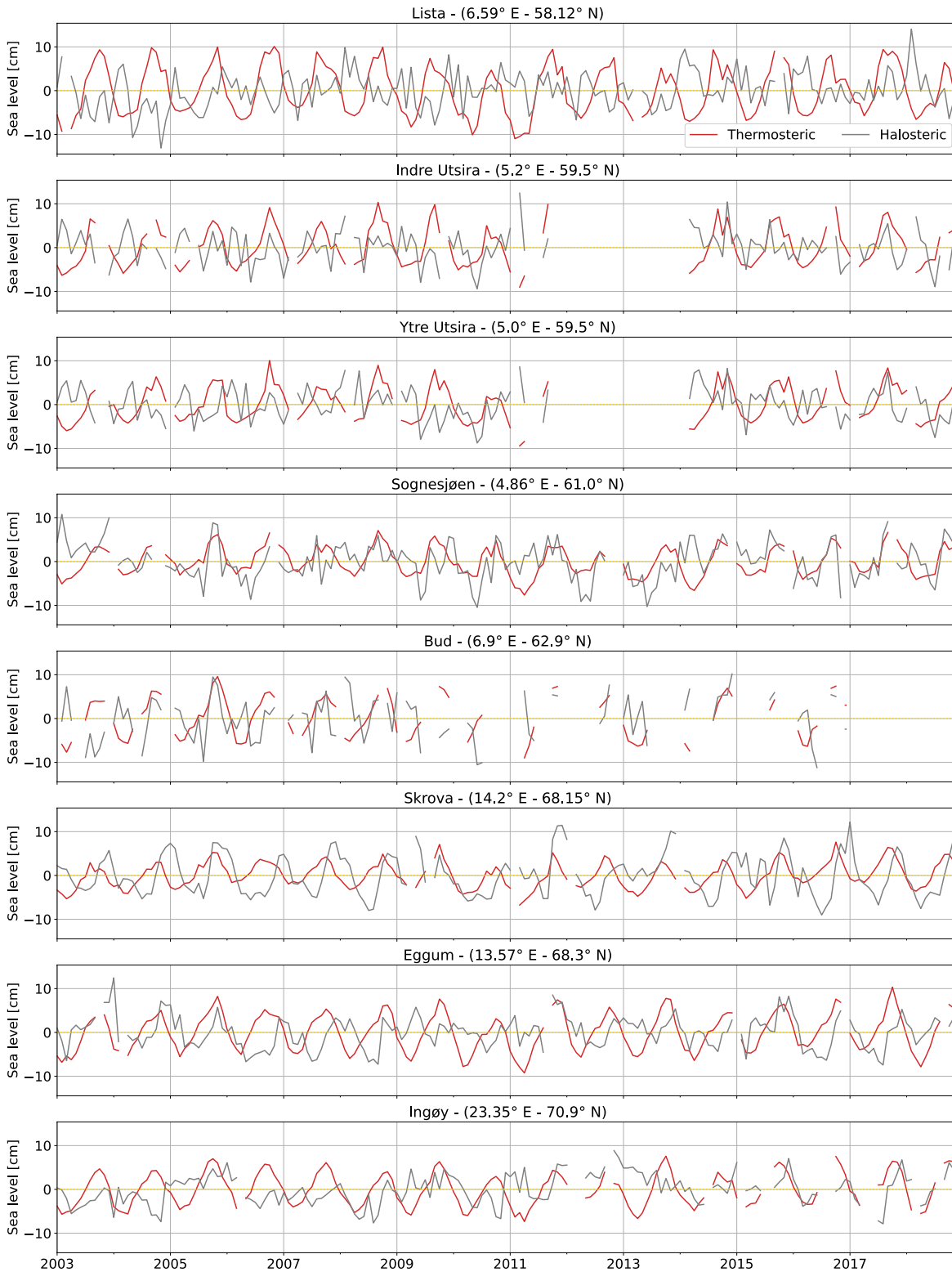
472

473 Despite these differences, both the thermosteric and the halosteric components of the sea level give a
474 comparable contribution to the sea-level variability along the Norwegian coast (Fig. 11). This ranges
475 approximately between -10 and 10 cm at each hydrographic station.

476

477 In the following sections, we investigate the spatial variability of these two components along the Norwegian
478 coast, focusing on the linear trend, the seasonal cycle, and the residuals, and on their contribution to the sea-
479 level variability in the region.

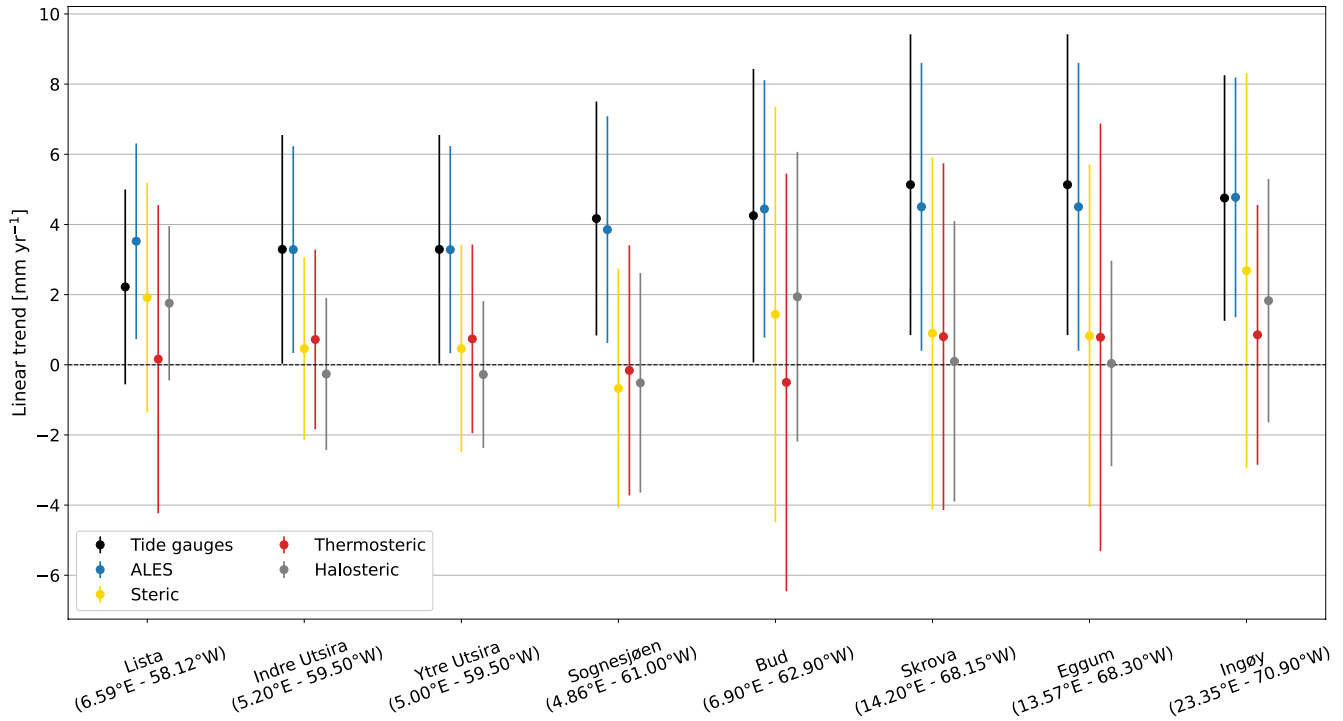
480



482 **Figure 11: Thermosteric (red) and halosteric (gray) components of the sea-level anomaly at each hydrographic station along the**
 483 **Norwegian coast.**
 484

485 **5.2 Steric contribution to the sea-level trend**

486



487 **Figure 12: At each hydrographic station, linear trend of the sea-level from tide gauges and from ALES (black and blue dots**
 488 **respectively), and of the steric, thermosteric and halosteric components of the sea level (yellow, red and gray dots respectively). The**
 489 **bars indicate the 95 % confidence intervals.**
 490

491

492 In this section, we perform a fit-for-purpose assessment of the Norwegian hydrographic station network to
 493 obtain estimates of the steric sea-level trends from satellite altimetry and in-situ data.

494

495 Over the period 2003-2018, we find that the linear trends of the thermosteric, halosteric and steric components
 496 of the sea level approximately range between -1.0 and 2.5 mm yr⁻¹. The steric contributions to coastal sea-level
 497 trends experience a large spatial variability, with it being even negative at Sognesjøen and reaching a peak of
 498 approximately 55% of the sea-level trend estimated from satellite altimetry at Lista and Ingøy. Moreover, when

499 we compare the thermosteric and the halosteric signals at these locations, we note that the latter contributes
500 more than the former to the coastal sea-level trends (up to 55% of the sea-level trend from altimetry). The
501 width of the confidence intervals of the thermosteric, halosteric and steric contributions ranges between 4.0
502 and 12.0 mm yr⁻¹ circa, with northern Norway exhibiting larger uncertainties (Fig. 12). This is a result of the high
503 inter-annual variability of the thermosteric and the halosteric components in the region (Figs. B1 and B4), which
504 leads to a fewer effective number of degrees of freedom and, therefore, to less accurate estimates of the linear
505 trend.

506

507 We also test if using tide gauges, instead of satellite altimetry, could alter our estimates of the relative
508 contribution of these components (thermosteric, halosteric and steric) to the sea-level trend along the coast of
509 Norway. Such alteration may indeed occur because the sea-level variations measured by the Norwegian tide
510 gauges might not properly represent those occurring in proximity of the hydrographic stations since the two
511 sets of instruments are not colocated in space (Fig. 1).

512

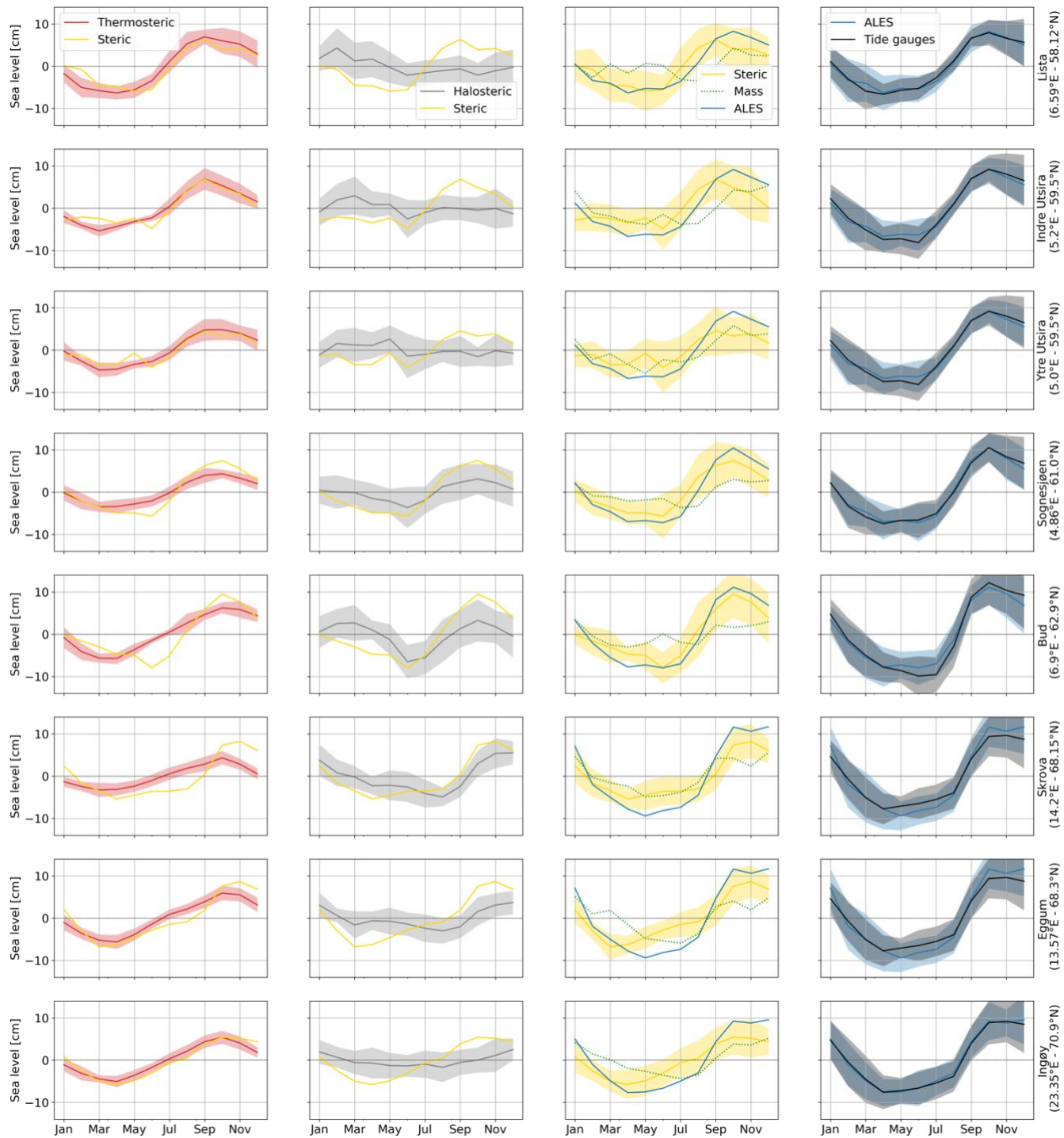
513 With the exception of Lista, the choice of the dataset has minimal influence on the estimates of the
514 thermosteric, halosteric and steric relative contributions to the sea-level trend along the coast of Norway. We
515 reach this conclusion by visual inspection, but we also provide a more quantitative analysis based on the ratio
516 between the linear-trend of the SLA and of the thermosteric, halosteric and steric components of the sea-level.
517 We find that, apart from Lista, the choice of the dataset modifies such a ratio by less than 13%. At Lista, the
518 change amounts to 59% and results from the ALES-retracked satellite altimetry dataset returning a sea-level
519 trend approximately 1.6 times larger than that provided by the tide gauge at Tregde (this is the tide gauge we
520 use to compute the thermohaline contribution at Lista). Such a large variation is expected since, as we have
521 already noticed, the sea-level rates obtained considering tide gauge and satellite data at Tregde show a less
522 accurate agreement (Figs. 9 and C5).

523

524

525 **5.3 Steric contribution to the seasonal cycle of sea level**

526



527
528
529

Figure 13: Monthly climatology of the sea-level signals at the hydrographic station positions. The panels show the steric (yellow lines), thermosteric (red lines), halosteric (gray lines), and mass (green lines) components of the sea-level. The monthly climatology obtained

530 from altimetry (blue lines) and tide-gauge (black lines) measurements are also shown. The shading enveloping the monthly
 531 climatologies shows the region departing from each line by one climatological standard deviation.

532

533

534

535

536

537

538

Table 1: Comparison between the seasonal cycle of SLA from ALES, of SLA from the tide gauges and of steric sea level at each hydrographic station position. The first and the second columns show, for ALES and the tide gauges, the RMSD between the seasonal cycle of SLA and of the steric sea-level, scaled by the range (maximum minus minimum) of the seasonal cycle of SLA. The third and the fourth columns show the ratio of the amplitudes and the lag of maximum correlation of the seasonal cycle of SLA from ALES and of steric sea level.

	Scaled $RMSD_{ALES}$	Scaled $RMSD_{Tide\ gauges}$	$\frac{Amplitude_{ALES}}{Amplitude_{Steric}}$	Lag maximum correlation ALES and steric (months)
Lista (6.59°E – 58.12°N)	16%	15%	0.8	1
Indre Utsira (5.20°E – 59.50°N)	21%	23%	0.7	1
Ytre Utsira (5.00°E – 59.50°N)	21%	22%	0.6	1
Sognesjøen (4.86°E – 61.00°N)	13%	14%	0.8	0
Bud (6.90°E – 62.90°N)	12%	16%	0.9	0
Skrova (14.20°E – 68.15°N)	18%	16%	0.7	0
Eggum (13.57°E – 68.30°N)	19%	14%	0.7	0
Ingøy (23.35°E – 70.90°N)	19%	19%	0.7	0

539

540

541

542 In this section, we build on the results by Richter et al. (2012), and assess the thermosteric, halosteric and steric
543 contributions to the seasonal cycle of the sea level at each hydrographic station along the Norwegian coast.

544

545 We find that using the tide gauge data, instead of satellite altimetry measurements, only little affects the
546 estimate of the thermosteric, halosteric and steric contributions to the seasonal cycle of SLA (Fig. 13), even
547 though the tide gauges are not colocated in space with the hydrographic stations. Indeed, the seasonal cycle
548 returned by satellite altimetry at each hydrographic station strongly resembles that returned by the nearby tide
549 gauge (Fig. 13, fourth column). At the same time, the RMSD between the seasonal cycle of the SLA and steric
550 sea level, scaled by the range (maximum minus minimum) of the seasonal cycle of SLA, little depends on the
551 dataset used (Table 1, first and second columns).

552

553 We also note that density changes contribute substantially to the seasonal cycle of SLA along the Norwegian
554 coast, as shown by Fig. 13 and Table 1. The seasonal cycle of SLA and steric sea-level are 1-month out-of-phase
555 along the southern and western coast of Norway up to Yndre-Utsira, and in-phase over the remaining part of
556 the Norwegian coast. Moreover, the ratio between the range of seasonal cycles of steric sea level and of SLA
557 varies between 0.6, at Ytre Utsira, and 0.9, at Bud (Table 1, third column).

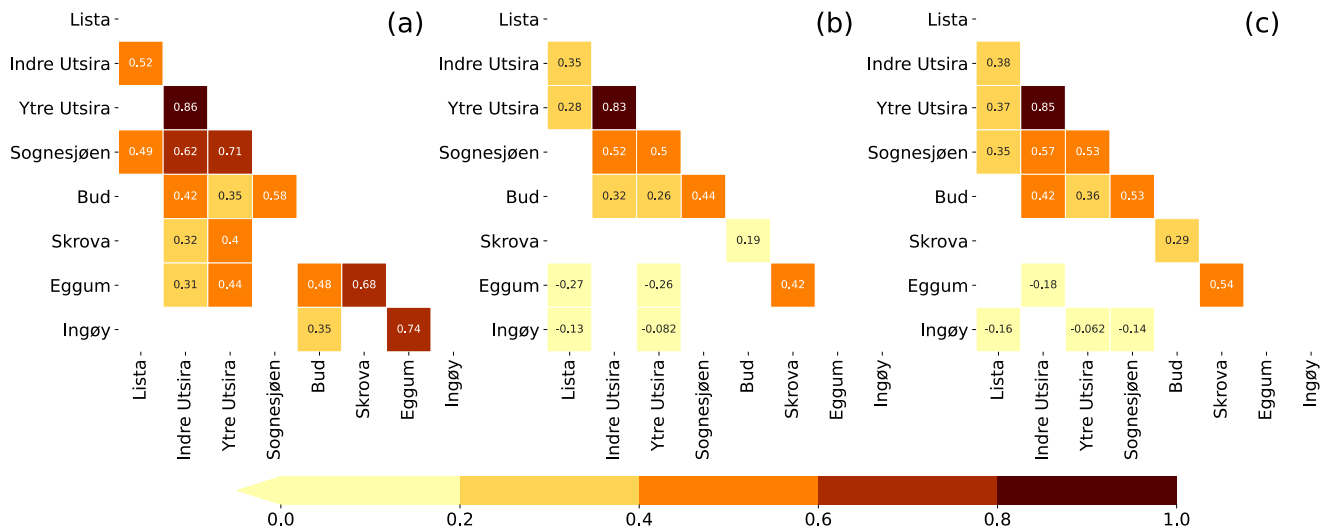
558

559 Along the Norwegian coast, the seasonal cycle of steric sea level is more affected by variations in temperature
560 than in salinity. We note that, with the exception of Bud and Skrova, the seasonal cycle of the steric component
561 mostly resembles that of the thermosteric component in terms of both amplitude and phase. At the same time,
562 we note a clear discrepancy between the seasonal cycle of the halosteric and steric components both in
563 southern Norway, where they are in anti-phase, and at Bud, where the seasonal cycle of the halosteric sea level
564 is dominated by the semi-annual cycle. A more quantitative analysis returns comparable results; the RMSD
565 between the steric and halosteric seasonal cycles exceeds by a factor of 1.4 the RMSD between the steric and
566 thermosteric seasonal cycles along the entire coast of Norway (with the exception of Skrova, where the ratio
567 between the two RMSDs is 0.7).

568

569

570 **5.4 Detrended and deseasoned coastal sea level and its components**



571
572 **Figure 14: Correlation matrices of the detrended and deseasoned thermosteric (a), halosteric (b) and steric (c) components of the sea level at each hydrographic station. Correlation values that are not significant at a 0.05 significance level have been omitted.**

574

575 The detrended and deseasoned thermosteric sea level along the Norwegian coast shows a larger spatial
576 variability compared to the detrended and deseasoned halosteric component (Fig. 14). The correlation matrix of
577 the thermosteric sea level (Fig. 14a) shows larger values compared to the one obtained considering the
578 halosteric sea-level signals (Fig. 14b). As an example, while the minimum linear correlation coefficient between
579 two adjacent hydrographic stations in Fig. 14a is 0.52, it is only 0.19 in Fig. 14b. We briefly discuss the small
580 spatial scale variability of the halosteric sea-level along the Norwegian coast in the Discussion and conclusions
581 section of the paper.

582

583 From Fig. 14c, we also note that the values of the correlation matrix of the steric sea-level fall in between those
584 of the thermosteric and of the halosteric components. This suggests that the thermosteric and halosteric
585 components of the sea-level give a similar contribution to the sea-level variability along the Norwegian coast.

586

587 **6 Discussion and conclusions**

588 In this paper, we have first assessed the ability of the ALES-reprocessed satellite altimetry dataset to capture
589 the Norwegian sea-level variability over a range of timescales. Then, we have used data from hydrographic
590 stations to quantify the steric contributions to the sea-level variability along the coast of Norway.

591

592 Along the Norwegian coast, the sea-level trend from the ALES-reprocessed satellite altimetry dataset is found to
593 be compatible with the estimates from tide gauges. Their difference only ranges between -0.85 and 1.15 mm yr⁻¹
594 and is significantly different from zero at the 95% confidence level at 19 out of 22 tide gauge locations.

595 Because of this good agreement, the choice of the sea-level dataset (either tide gauges or ALES) has minimal
596 impact on the estimates of the thermosteric, of the halosteric and of the steric relative contributions to the sea-
597 level trend. Despite the large uncertainties, this result is encouraging since it suggests that the ALES dataset can
598 be used to partition the sea-level variability in regions of the coastal ocean not covered by tide gauges. At the
599 same time, it confirms the validity of previous sea-level studies in the region which only used tide gauge data
600 (e.g., Richter et al., 2012).

601

602 Regarding the comparison between the ALES-retracked and the along-track (L3) conventional altimetry
603 datasets, we find that the former shows, on average, a 6% improvement, despite it being well within the
604 margins of error. This improvement is most evident at Bodø, Kabelvåg and Tromsø, in northern Norway, where
605 the agreement with the tide gauges improves by 19%, 23% and 24% respectively. The use of the ALES retracker
606 to more satellite altimetry missions, in order to have more observations and to cover the period before July
607 2002, might help reduce the uncertainties and return a more statistically significant result.

608

609 A comparison with Breili et al. (2017), where an along-track (L3), multi-mission conventional altimetry dataset
610 was used to analyse the sea-level trend along the Norwegian coast, returns comparable results. We cannot,
611 however, directly compare the linear trends in this work with those in Breili et al. (2017) since they focus on a
612 different period (1993-2016), and the sea-level trend along the Norwegian coast strongly depends on the length
613 of the time-window considered (Fig. 10). However, when assessing how the conventional satellite altimetry
614 datasets compare with tide-gauge records in terms of linear trend computed over a common time-window,

615 ALES shows again an improvement in northern Norway, between Bodø and Tromsø, where the difference
616 between the linear trend from ALES and the tide gauges are small (up to 0.5 mm yr^{-1}), compared to circa 1 to 3
617 mm yr^{-1} found by Breili et al. (2017) using a conventional altimetry dataset.

618

619 The ALES-retracked satellite altimetry dataset is found to underestimate the amplitude of the annual cycle
620 along large portions of the Norwegian coast (Fig. 7). Even though the difference between the two sets of
621 estimates is not significant at a 95% significance level (the 95% confidence interval is approximately twice the
622 standard error), we find this result interesting because of its consistency. We do not expect such a consistency
623 to depend on the ALES retracker since we find a comparable result when we use the along-track (L3)
624 conventional altimetry product (Fig. C3). We rather suspect a dependence of the amplitude of the annual cycle
625 on the bathymetry and, therefore, on the distance from the coast, as shown by Passaro et al. (2015) along the
626 Norwegian sector of the Skagerrak.

627

628 A comparison with Volkov and Pujol (2012) shows that the ALES-retracked satellite altimetry better captures the
629 sea-level annual cycle along the coast of Norway with respect to the gridded sea-level altimetry products. In
630 that study, the authors have considered six tide gauges along the Norwegian coast, namely, Kristiansund,
631 Rørvik, Andenes, Hammerfest, Honningsvåg and Vardø to assess the quality of satellite altimetry maps at the
632 northern high latitudes. Except for Andenes, we note that the ALES-reprocessed coastal altimetry dataset allows
633 for more accurate estimates of the sea-level annual cycle, reducing the differences with the in situ sea-level
634 records by a factor of 3 to 6 compared to gridded satellite altimetry products.

635

636 We also assess the steric contribution to the seasonal cycle of SLA. Our results show that the steric variations
637 and, in particular, the thermosteric variations contribute considerably to the seasonal cycle of the sea level
638 along the entire Norwegian coast. Moreover, we find that the relative contributions of the thermosteric,
639 halosteric and steric sea level little depends on whether we use tide gauges or satellite altimetry. This is
640 indicative of the large-scale spatial pattern associated with the seasonal cycle of SLA.

641

642 The detrended and deseasoned sea-level variability along the Norwegian shelf resembles the along-slope wind
643 index proposed by Chafik et al. (2019). We note that the similarities between the two are stronger along the

644 western and the northern coast of Norway than in the south. Indeed, from Oslo to Ålesund, those SLA signals
645 depart from the along-slope winds index between 2003 and 2008, probably due to local effects, such as the
646 Baltic outflow. We refer to local effects since Chafik et al. (2019) attributed the interannual sea-level variability
647 over the northern European continental shelf to the along-slope winds, which might regulate the exchange of
648 water between the open ocean and the shelf through Ekman transport.

649
650 Because the detrended and deseasoned SLA pattern is coherent over large distances along the Norwegian coast
651 (see also Chafik et al., 2017), coastal altimetry observations located a few hundred kilometres apart can be
652 representative of the sea-level variations occurring at a particular tide gauge location. This explains why we can
653 average the SLA from altimetry over an area a few hundreds of kilometres wide around each tide gauge location
654 to maximize the linear correlation coefficient between the detrended and deseasoned SLA from satellite
655 altimetry and the tide gauges (Section 3.2). Moreover, it also partly explains the good agreement between
656 satellite altimetry and tide gauges since, as we average over a large number of satellite altimetry observations,
657 we increase the temporal sampling provided by altimetry and, therefore, we reduce the noise in the resulting
658 SLA (Oelsmann et al., 2021).

659
660 The small-scale variability of the detrended and deseasoned sea-level halosteric component (Fig. 14) does not
661 reconcile with the good agreement between tide gauge sea-level signals and the ALES-reprocessed altimetry
662 dataset. Indeed, to compare the two datasets, we have averaged the satellite altimetry observations over an
663 area a few hundreds of kilometres wide around each tide gauge. However, Figure 14 suggests that the
664 estimates of the halosteric component can change significantly over an area of this size. Furthermore, while this
665 component has a magnitude comparable to that of the detrended, deseasoned SLA (not shown), it only explains
666 a small fraction (from 3 to 11 %) of the difference between the sea-level signals from altimetry and the tide
667 gauges.

668
669 Future work is thus warranted to understand whether the small-scale variability of the halosteric component of
670 the sea-level along the Norwegian coast results from measurement issues. For example, ocean salinity is
671 measured approximately once a week at Skrova and approximately twice a month at the remaining
672 hydrographic stations: this aliases the sub-weekly salinity variations into the lower frequency components and,

673 consequently, might significantly alter the monthly mean salinity values. A new study, which takes benefit from
674 ships of opportunity, synergies between different observational platforms and ocean models, could help clarify
675 this issue.

676

677 To conclude, we have demonstrated the advantage of the ALES-retracker over the conventional open ocean
678 retracker along the coast of Norway. The retracking of earlier altimeter missions would, however, be necessary
679 to provide a more accurate estimate of the sea-level variability along the coast of Norway and possibly used to
680 understand whether the sea-level in the region is accelerating. Still, this paper gives confidence that the ALES-
681 reprocessed altimetry dataset can be fruitfully used to measure coastal sea-level variations in regions poorly
682 covered by tide gauges.

683

684

685 **Appendix A**

686 To estimate the uncertainty associated with the sea-level trends derived from tide gauges and the ALES-
687 retracked satellite altimetry dataset (Fig. 9), we need to account for the effective degrees of freedom in the sea-
688 level anomaly time series. Indeed, successive points in the SLA time series might be correlated and, therefore,
689 not drawn from a random sample.

690

691 To determine the effective number of degrees of freedom, we produce the semi-variograms of the detrended
692 and deseasoned SLA from the tide gauges and the altimetry dataset. The semi-variogram is defined as:

693

$$694 \gamma(t) = \frac{1}{2} \cdot \text{var}[x(t) - x(t + \tau)] \quad (4)$$

695

696 where $x(t)$ is the time series under study, var stands for variance, and τ is the time lag.

697

698 The number of degrees of freedom is obtained by fitting the semi-variograms with a spherical function of the
699 form:

700

$$\begin{cases} c(h) = b + C_0 \cdot \left(1 - \frac{3|h|}{2a} + \frac{1|h|^3}{2a^3}\right) & \text{if } h \leq a \\ c(h) = b + C_0 & \text{if } h > a \end{cases} \quad (5)$$

702

703 where h is the fitting parameter, and a is the effective range or, in other words, the lag needed for the semi-
704 variogram to reach a constant value. Semi-variograms are preferred to autocorrelations in geostatistics because
705 they better detect the non-stationarity of time series.

706

707 We use the fit to determine the lag at which each semi-variogram reaches a plateau, since it indicates the
708 decorrelation timescale of the time series. The effective number of degrees of freedom corresponds to the ratio
709 between the length of the time series and the lag.

710

711 We find that the lag only little depends on the tide gauge location, and on whether we consider the detrended
712 and deseasoned SLA from the altimetry dataset or the tide gauges (Figs. A1 and A2). The semi-variograms
713 obtained from both altimetry and the tide gauges return a lag of 2 months at each tide gauge location, with the
714 exception of three stations in southern Norway (Viker, Oscarborg and Helgeroa), where the SLA from the tide
715 gauges is characterized by a 3-month lag.

716

717 We use the same approach to compute the uncertainty associated with the linear trend of the difference
718 between the SLA from satellite altimetry and the tide gauges, with only one exception. We noticed that the
719 spheric model does not fit the semi-variogram for Trondheim. Therefore, for Trondheim, we opted for an
720 exponential model:

721

$$\gamma(t) = b + C_0 \left(1 - e^{-\frac{h}{a}}\right)$$

723 (6)

724

725 where h the fitting parameter, and a is the range parameter. An exponential function is preferred over the
726 spherical function when the time series shows a strong temporal correlation.

727

728 The serial correlation is negligible along the entire Norwegian coast with the exception of Viker, Oscarborg, Oslo
729 and Narvik, where the semi-variograms return a 2-month lag (Fig. A3). At Trondheim, instead, we find a much
730 larger lag (approximately 10 months).

731

732 We use the effective number of degrees of freedom when we compute the confidence intervals of the sea-level
733 rates in Fig. 9. We compute the 95% confidence interval of the linear trend as follows:

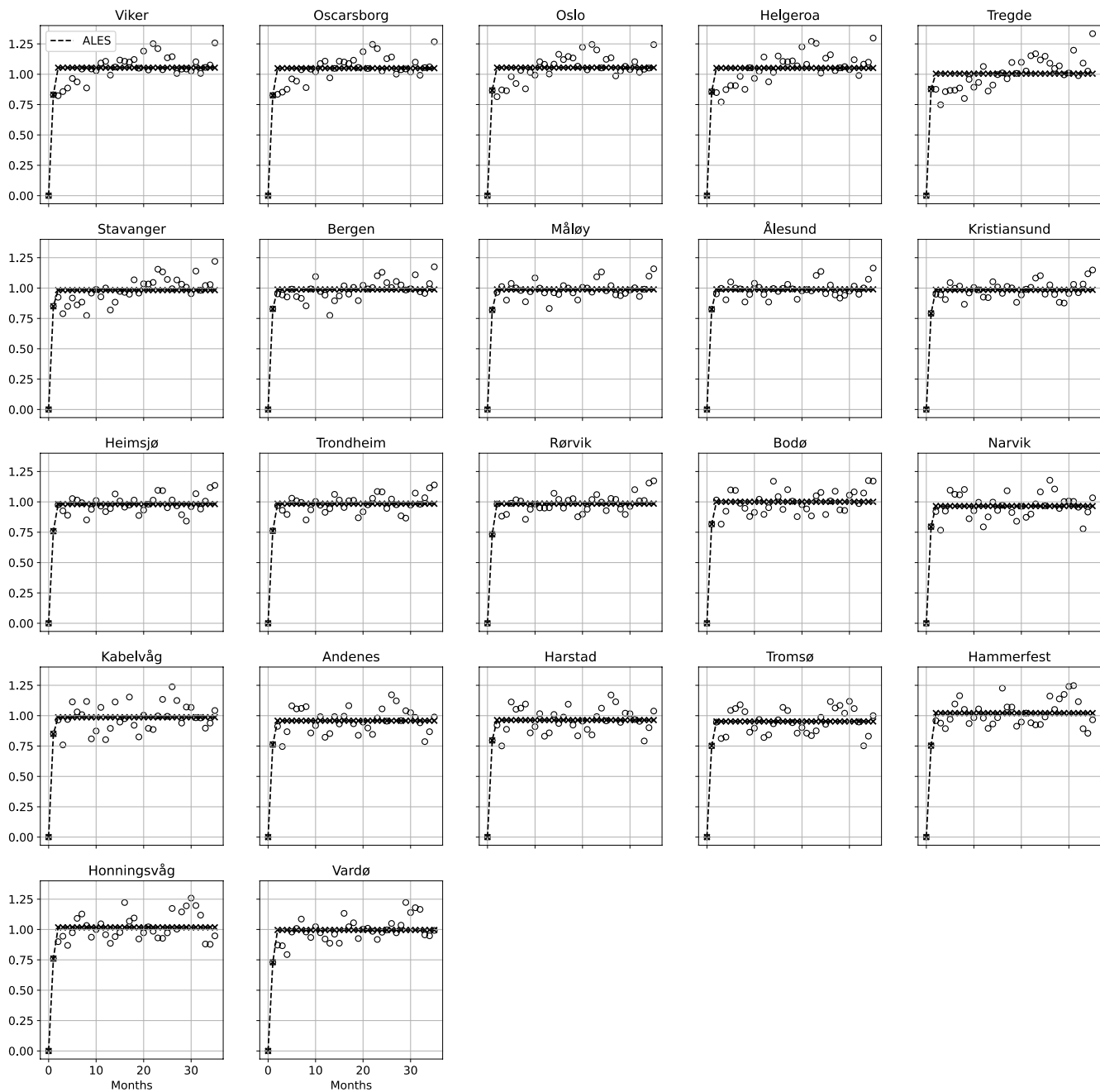
734

$$735 \quad CI = t_{0.05/2, N^*-6} \cdot \sqrt{\frac{N-1}{N^*-1}} \cdot SE \quad (7)$$

736

737 where SE is the standard error of the linear trend, computed as if $N^* = N$, the total number of observations in
738 the time series, and $t_{0.05/2, N^*-6}$ is the t-values computed using $N^* - 6$ degrees of freedom at a 0.05
739 significance level.

740

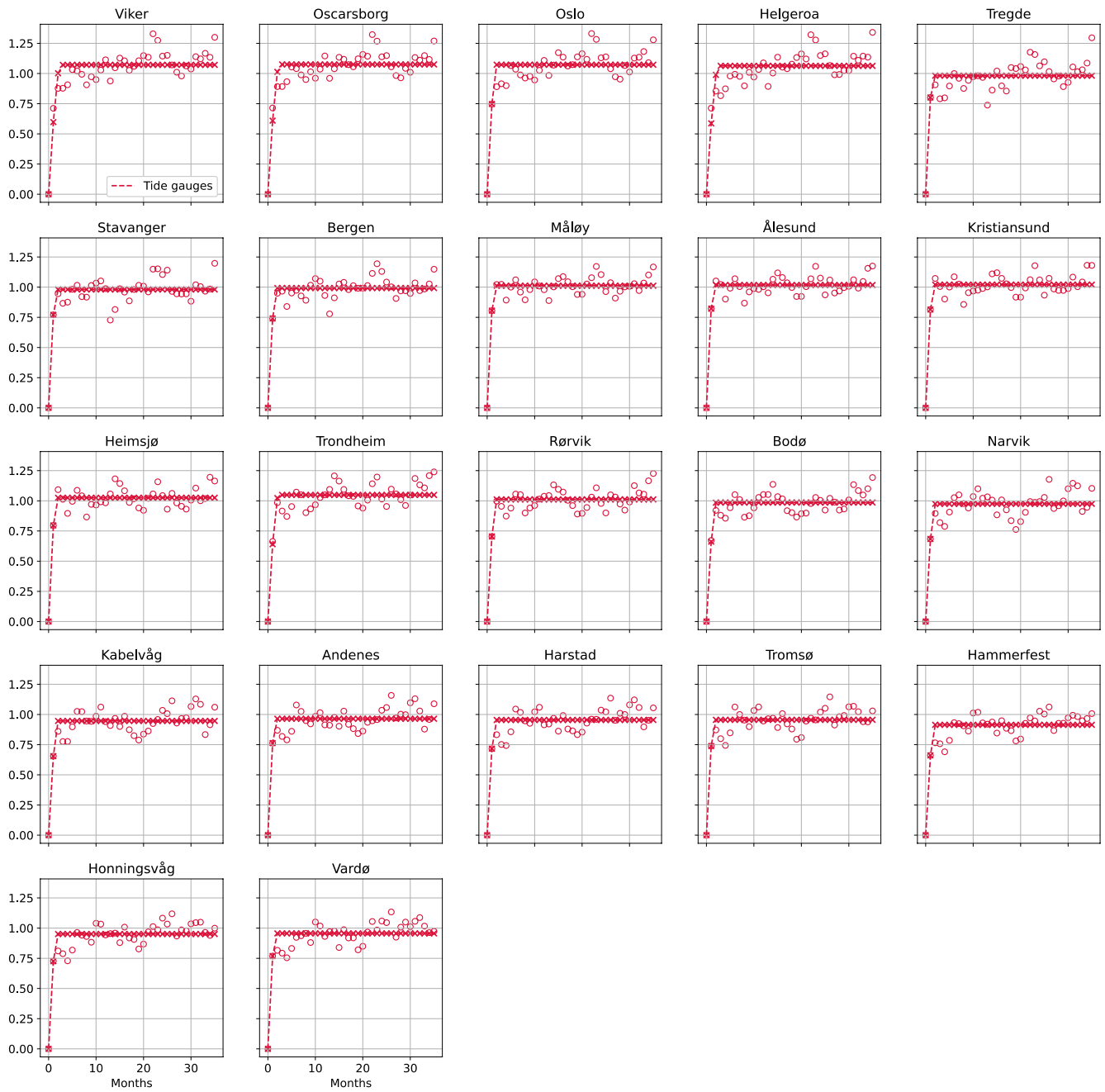


741
742
743
744
745
746

Figure A1: For each tide gauge along the Norwegian coast, semi-variogram of the detrended and deseasoned SLA estimated from the ALES-retracker satellite altimetry (empty circles) and corresponding fit (crosses connected by a dashed line). At each tide gauge location, we scaled each semi-variogram by the variance of the corresponding detrended and deseasoned SLA for all the plots to have the same limits on the y axis.

747

748



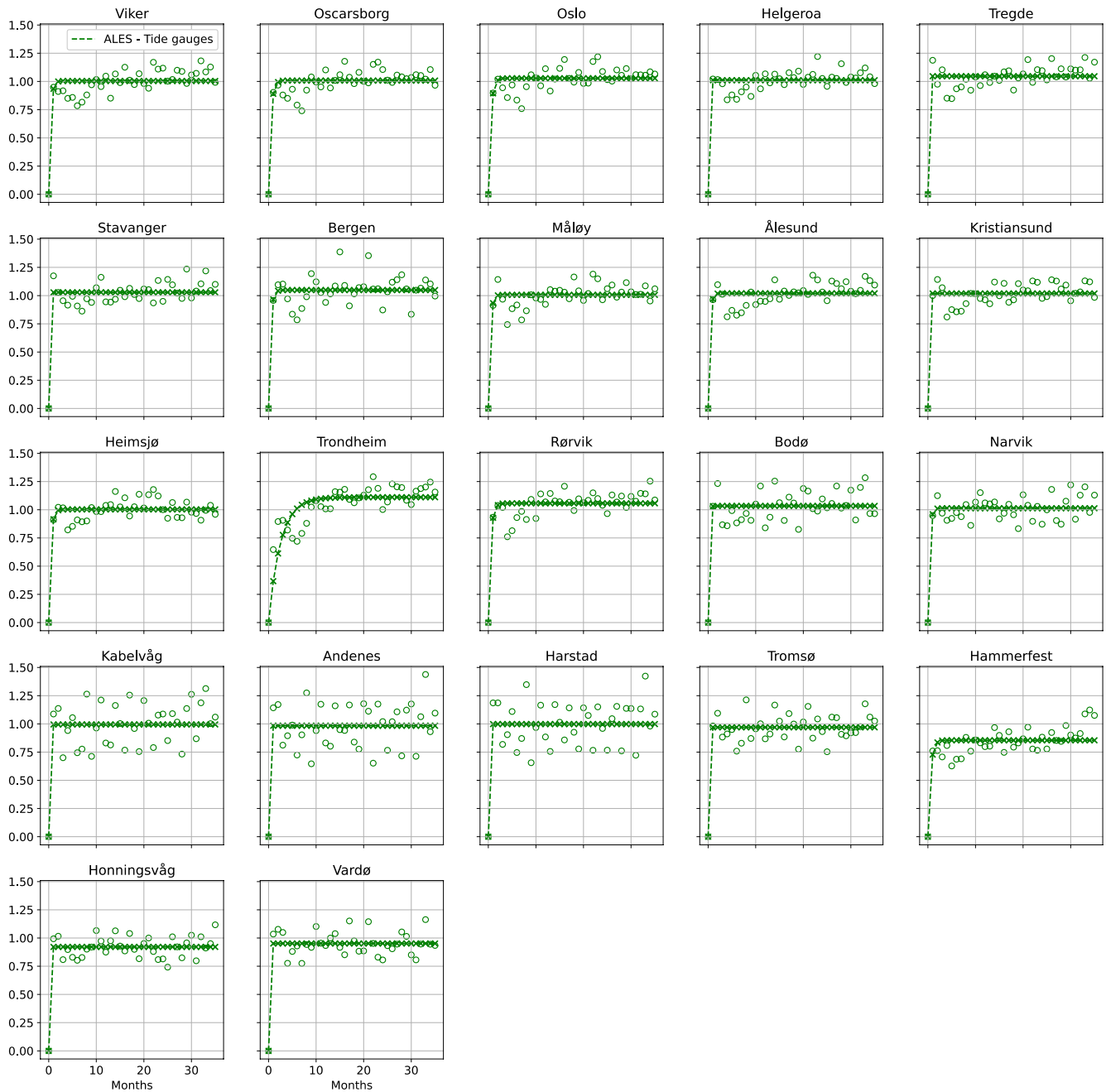
749

750

751

Figure A2: For each tide gauge along the Norwegian coast, semi-variogram of the detrended and deseasoned SLA measured by the tide gauge (empty circles) and corresponding fit (crosses connected by a dashed line). At each tide gauge location, we scaled each

752 semi-variogram by the variance of the corresponding detrended and deseasoned SLA for all the plots to have the same limits on the y
753 axis.
754
755
756



757

758

759

760

761

762

763

Figure A3: For each tide gauge along the Norwegian coast, semi-variogram of the difference between the detrended and deseasoned SLA estimated from the ALES-retracker satellite altimetry and the tide gauge (empty circles) and corresponding fit (crosses connected by a dashed line). At each tide gauge location, we scaled each semi-variogram by the variance of the corresponding detrended and deseasoned SLA for all the plots to have the same limits on the y axis.

764 **Appendix B**

765

766 Following the same argument as in the Appendix A of the Supplementary Material, to estimate the uncertainty
767 associated with the linear trends of the thermosteric, of the halosteric and of the steric components of the sea-
768 level along the Norwegian coast (Fig. 12), we need to account for the effective degrees of freedom in the
769 corresponding time series.

770

771 As in Section A of the Supplementary Material, to determine the effective number of degrees of freedom, we
772 first produce the semi-variograms of the detrended and deseasoned thermosteric, of the halosteric and of the
773 steric components of the sea-level at each hydrographic station. Then, we determine the time needed by the
774 semi-variogram's fit to approximately reach a plateau, adopting an exponential function (See Appendix A).

775

776 The thermosteric sea-level (Fig. B1) shows the strongest serial correlation. The semi-variogram of the
777 thermosteric sea-level returns lags ranging from 3 months, at Indre Utsira, to around 20 months at Skrova. In
778 general, the thermosteric component of the sea-level in northern Norway has fewer degrees of freedom than in
779 the south.

780

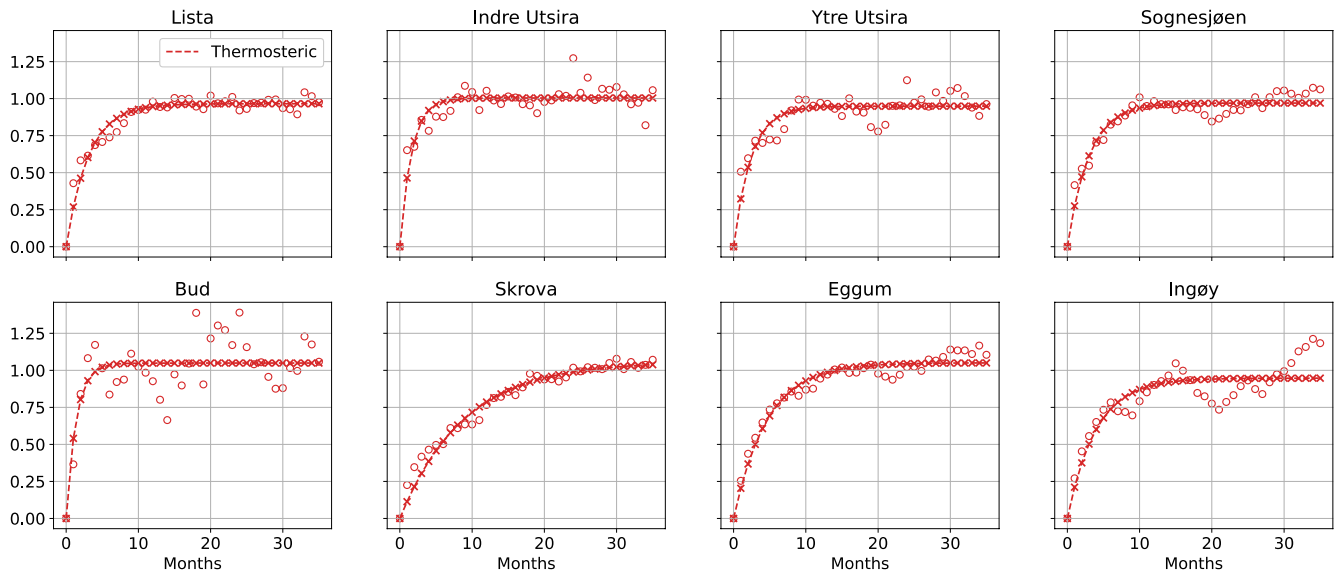
781 The halosteric (Fig. B2) and the steric (Fig B3) components show a similar pattern, with the number of effective
782 degrees of freedom being smaller in the north than in the south. However, both components show a weaker
783 serial correlation when compared to the thermosteric component of the sea-level. Indeed, the semi-variograms
784 return lags between 3 and 9 months for both components of the sea-level.

785

786 Similarly to the Appendix A, we use formula (7) to compute the 95% confidence interval of the linear trend of
787 the SLA and of the thermosteric, halosteric and steric components of the sea-level at each hydrographic station.
788 With respect to (7) though, here we only consider $N^* - 2$ degrees of freedom since the linear model that we
789 use to fit the time series has only two parameters (the offset and the angular coefficient of the straight line).

790

791



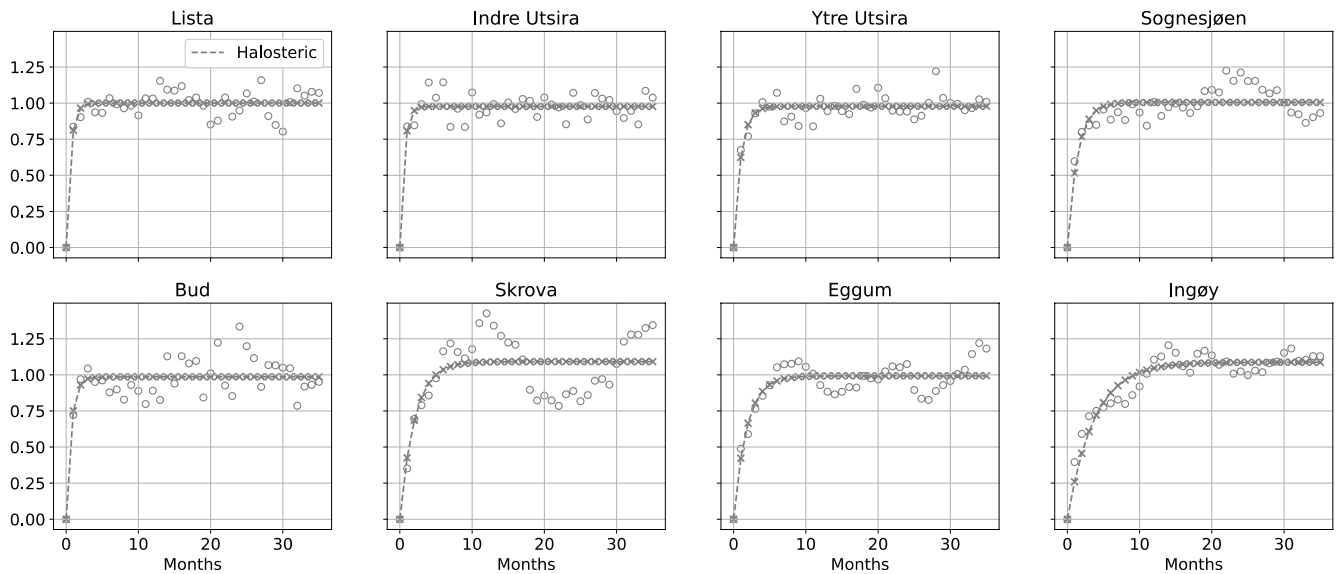
792

793 **Figure B1: For each hydrographic station along the Norwegian coast, semi-variogram of the detrended and deseasoned thermosteric**
 794 **component of the sea-level variability (empty circles) and corresponding fit (crosses connected by a dashed line). At each**
 795 **hydrographic station location, we scaled each semi-variogram by the variance of the corresponding detrended and deseasoned**
 796 **thermosteric component of the sea-level for all the plots to have the same limits on the y axis.**

797

798

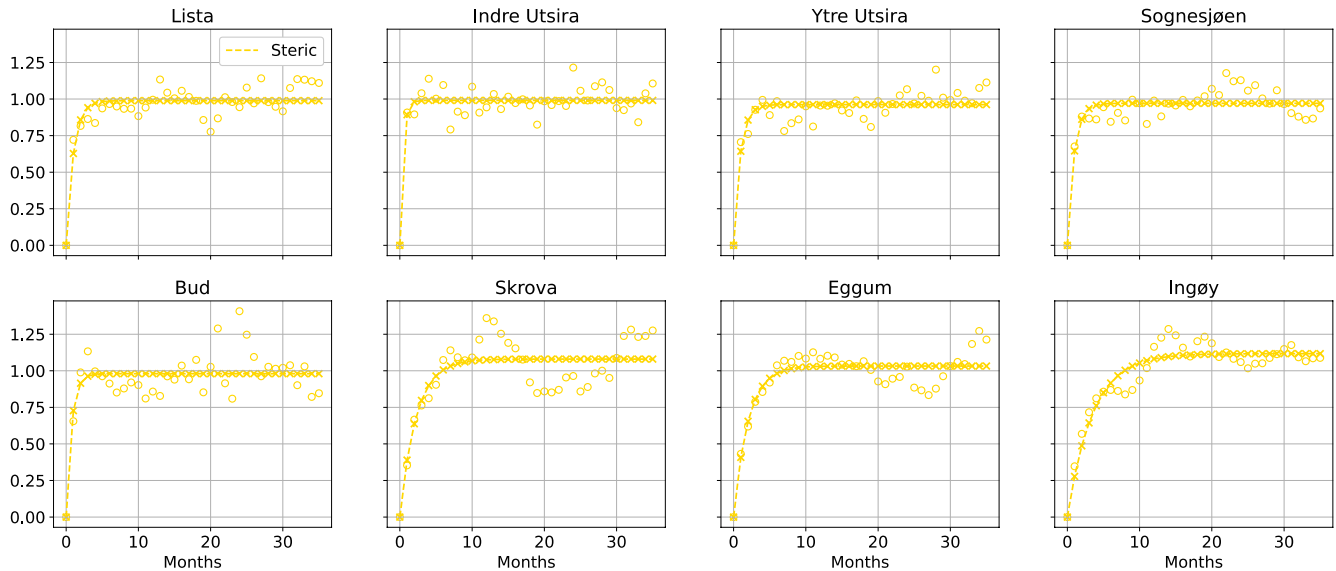
799



800

801 **Figure B2: For each hydrographic station along the Norwegian coast, semi-variogram of the detrended and deseasoned halosteric**
 802 **component of the sea-level variability (empty circles) and corresponding fit (crosses connected by a dashed line). At each**

803 hydrographic station location, we scaled each semi-variogram by the variance of the corresponding detrended and deseasoned
804 halosteric component of the sea-level for all the plots to have the same limits on the y axis.
805
806
807



808
809 **Figure B3:** For each hydrographic station along the Norwegian coast, semi-variogram of the detrended and deseasoned steric
810 component of the sea-level variability (empty circles) and corresponding fit (crosses connected by a dashed line). At each
811 hydrographic station location, we scaled each semi-variogram by the variance of the corresponding detrended and deseasoned steric
812 component of the sea-level for all the plots to have the same limits on the y axis.
813
814

815 Appendix C

816
817 To compare the performance of the ALES-retracked and the conventional satellite altimetry dataset, we have
818 download the along-track L3 satellite altimetry missions provided on the Copernicus website:

819
820 [https://resources.marine.copernicus.eu/product-](https://resources.marine.copernicus.eu/product-download/SEALEVEL_GLO_PHY_L3_REP_OBSERVATIONS_008_062)
821 [download/SEALEVEL_GLO_PHY_L3_REP_OBSERVATIONS_008_062](https://resources.marine.copernicus.eu/product-download/SEALEVEL_GLO_PHY_L3_REP_OBSERVATIONS_008_062).

822
823 even though we should remember that the discrepancy between the two datasets might not only result from
824 the different retracers, but also from the different geophysical corrections applied to the data.

825

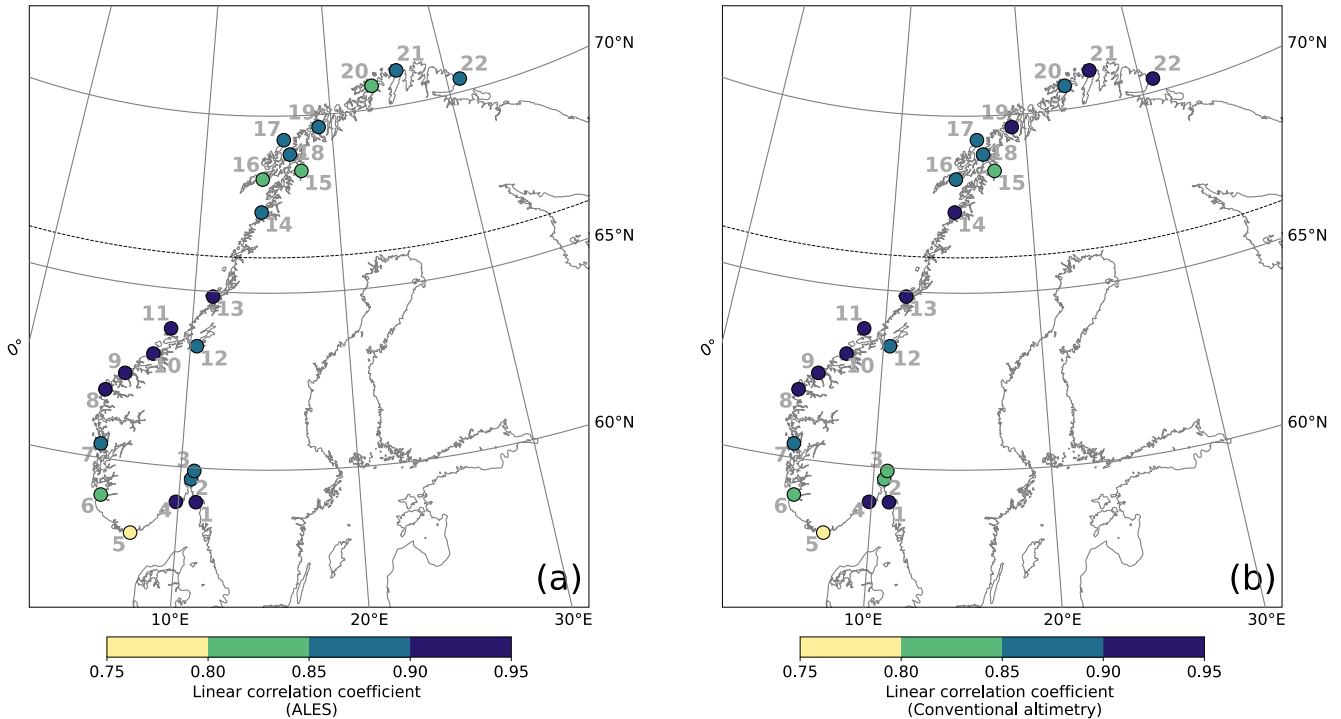
826

827 We select the same satellite altimetry missions that have been reprocessed with the ALES-retracker and we

828 make sure that both satellite altimetry datasets cover the same period.

829

1 - Viker	4 - Helgeroa	7 - Bergen	10 - Kristiansund	13 - Rørvik	16 - Kabelvåg	19 - Tromsø	21 - Honningsvåg
2 - Oscarsborg	5 - Tregde	8 - Måløy	11 - Heimsjø	14 - Bodø	17 - Andenes	20 - Hammerfest	22 - Vardø
3 - Oslo	6 - Stavanger	9 - Ålesund	12 - Trondheim	15 - Narvik	18 - Harstad		



830

831 **Figure C1: Comparison between coastal sea-level signals from in situ measurements and the area-averaged ALES-reprocessed satellite**

832 **altimetry dataset and the conventional satellite altimetry dataset. At each tide gauge location, linear correlation coefficient between**

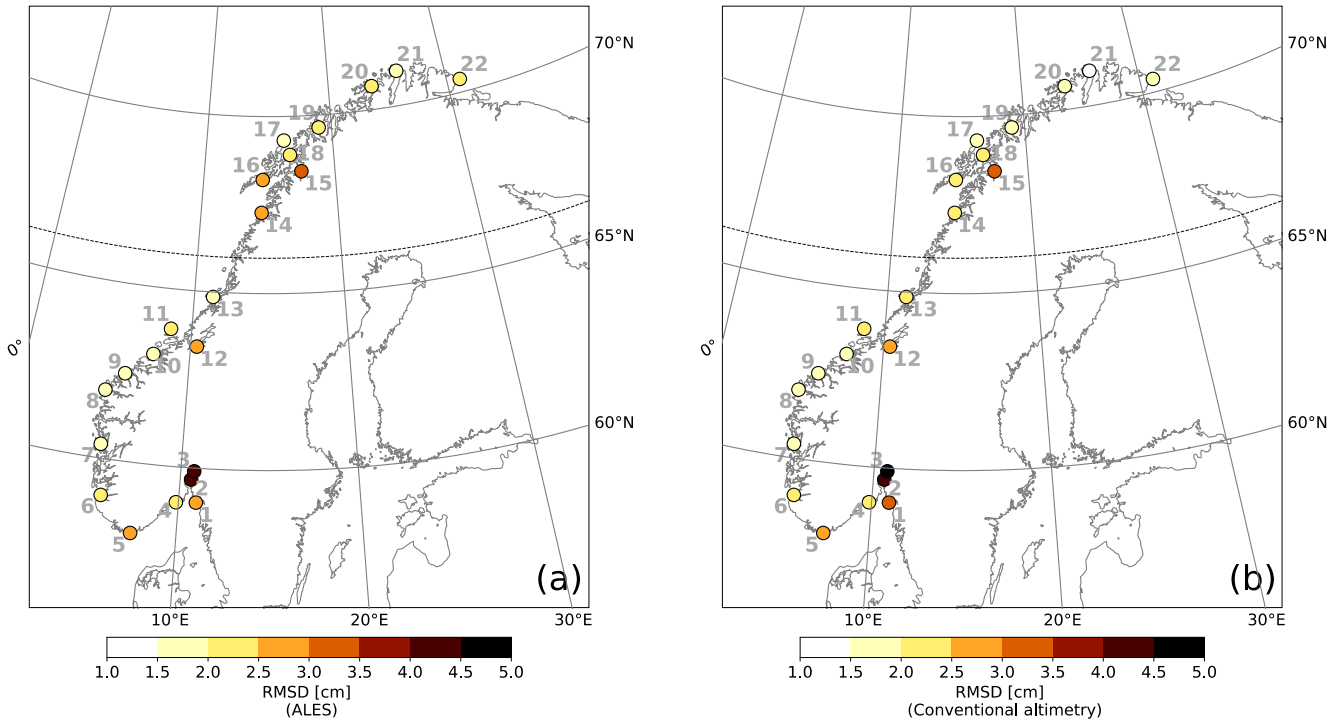
833 **the detrended and deseasoned monthly mean SLA from the ALES-reprocessed satellite altimetry dataset and from the tide gauge (a),**

834 **and from the conventional altimetry dataset and the tide gauge. The black, dashed line indicates the 66°N parallel.**

835

836

1 - Viker	4 - Helgeroa	7 - Bergen	10 - Kristiansund	13 - Rørvik	16 - Kabelvåg	19 - Tromsø	21 - Honningsvåg
2 - Oscarsborg	5 - Tregde	8 - Måløy	11 - Heimsjø	14 - Bodø	17 - Andenes	20 - Hammerfest	22 - Vardø
3 - Oslo	6 - Stavanger	9 - Ålesund	12 - Trondheim	15 - Narvik	18 - Harstad		

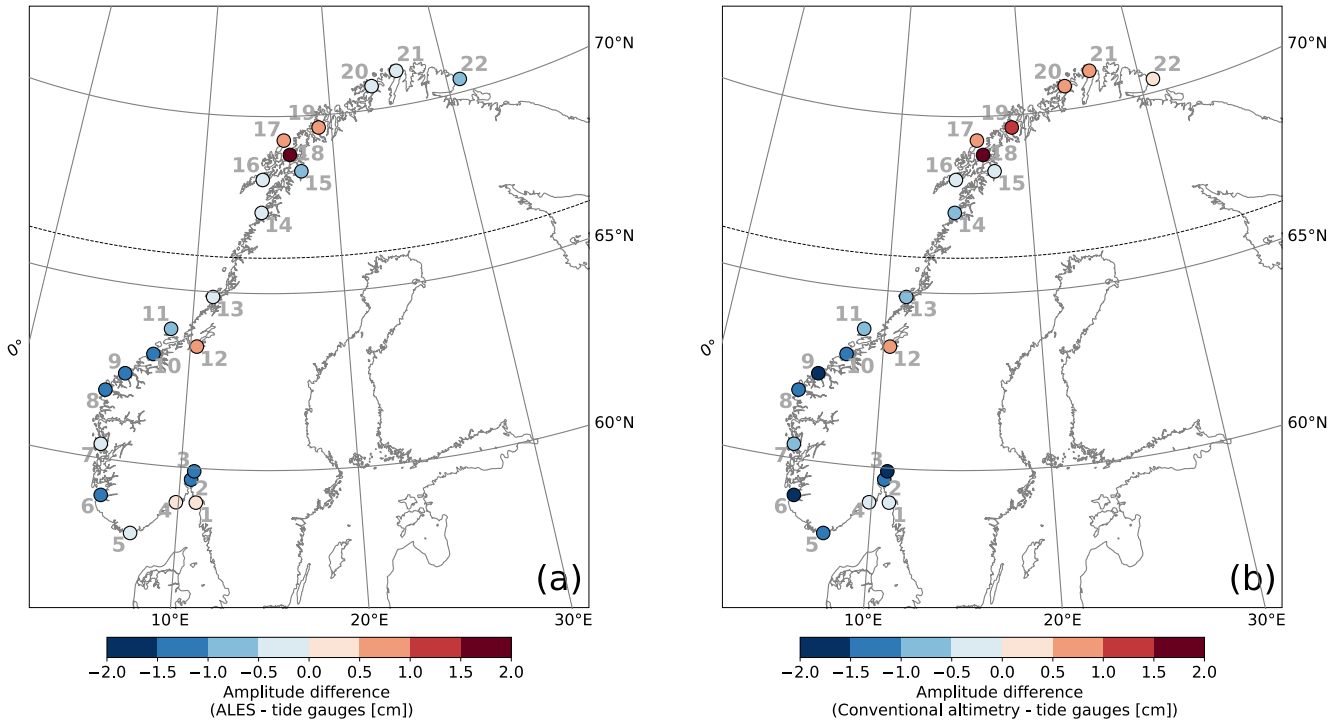


837

838 **Figure C2: Comparison between coastal sea-level signals from in situ measurements and the area-averaged ALES-reprocessed satellite**
 839 **altimetry dataset and the conventional satellite altimetry dataset. At each tide gauge location, RMSD of the detrended and**
 840 **deseasoned monthly mean SLA from the ALES-reprocessed satellite altimetry dataset and from the tide gauge (a), and from the**
 841 **conventional altimetry dataset and the tide gauge. The black, dashed line indicates the 66°N parallel.**
 842

843

1 - Viker	4 - Helgeroa	7 - Bergen	10 - Kristiansund	13 - Rørvik	16 - Kabelvåg	19 - Tromsø	21 - Honningsvåg
2 - Oscarsborg	5 - Tregde	8 - Måløy	11 - Heimsjø	14 - Bodø	17 - Andenes	20 - Hammerfest	22 - Vardø
3 - Oslo	6 - Stavanger	9 - Ålesund	12 - Trondheim	15 - Narvik	18 - Harstad		



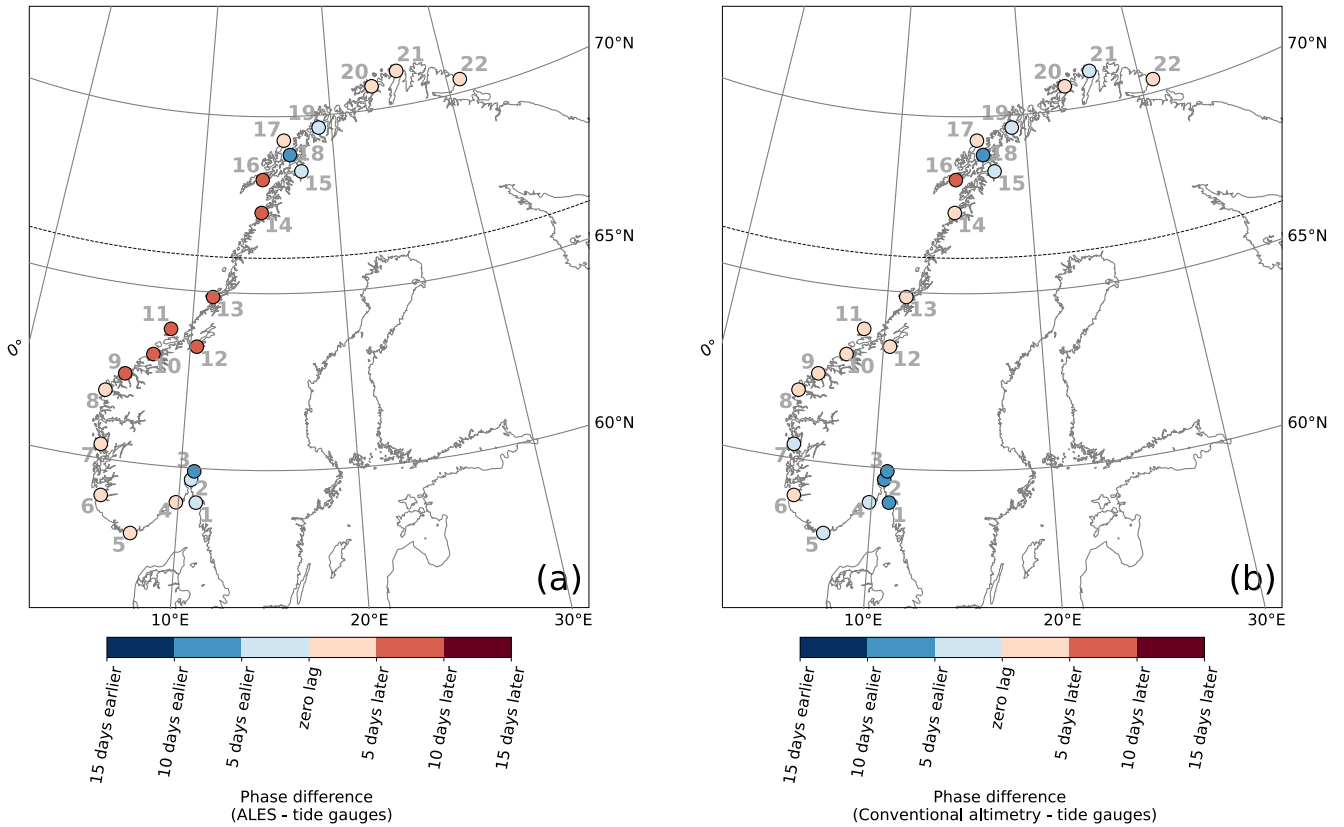
844

845 **Figure C3: Comparison between coastal sea-level signals from in situ measurements and the area-averaged ALES-reprocessed satellite**
 846 **altimetry dataset and the conventional satellite altimetry dataset. At each tide gauge location, difference between the amplitude of**
 847 **the annual cycle from the ALES-reprocessed altimetry dataset and the tide gauge (a), and from the conventional altimetry dataset and**
 848 **the tide gauge (b). The black, dashed line indicates the 66°N parallel.**
 849

850

851

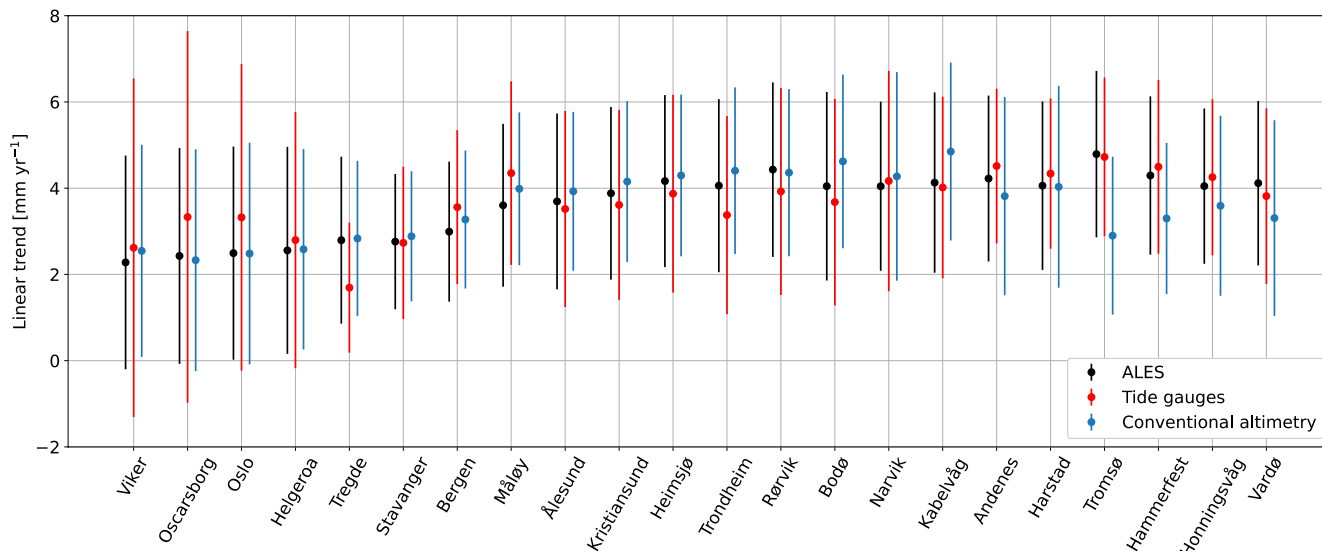
1 - Viker	4 - Helgeroa	7 - Bergen	10 - Kristiansund	13 - Rørvik	16 - Kabelvåg	19 - Tromsø	21 - Honningsvåg
2 - Oscarsborg	5 - Tregde	8 - Måløy	11 - Heimsjø	14 - Bodø	17 - Andenes	20 - Hammerfest	22 - Vardø
3 - Oslo	6 - Stavanger	9 - Ålesund	12 - Trondheim	15 - Narvik	18 - Harstad		



852

853 **Figure C4: Comparison between coastal sea-level signals from in situ measurements and the area-averaged ALES-reprocessed satellite**
854 **altimetry dataset and the conventional satellite altimetry dataset. At each tide gauge location, difference between the phase of the**
855 **annual cycle from the ALES-reprocessed altimetry dataset and the tide gauge (a), and from the conventional altimetry dataset and the**
856 **tide gauge (b). The black, dashed line indicates the 66°N parallel.**

857



858
859
860
861
862

Figure C5: At each tide gauge location, linear trend of the SLA from the ALES-reprocessed altimetry dataset (black dots), from conventional altimetry dataset (cyan dots) and from tide gauges (red dots). The error bars show the 95th confidence intervals of the sea-level trend at each tide gauge location.

863
864

865 Data availability

866 The tide gauge data are available and distributed through a dedicated web API (api.sehavniva.no). The ALES SSH
867 data were produced by DGF1-TUM and distributed via OpenADB (<http://www.openadb.dgfi.tum.de>). More
868 details on the retracker and the product are available in Passaro et al. (2014), Passaro et al. (2015) and Passaro
869 et al, (2017). The conventional altimetry dataset can be accessed from the Copernicus website at
870 [https://resources.marine.copernicus.eu/product-](https://resources.marine.copernicus.eu/product-download/SEALEVEL_GLO_PHY_L3_REP_OBSERVATIONS_008_062)
871 [download/SEALEVEL_GLO_PHY_L3_REP_OBSERVATIONS_008_062](https://resources.marine.copernicus.eu/product-download/SEALEVEL_GLO_PHY_L3_REP_OBSERVATIONS_008_062). The hydrographic stations dataset are
872 updated and available at <http://www.imr.no/forskning/forskningsdata/stasjoner/index.html>.

873
874
875

Author contribution

876 FM, AB, LC and LB designed the research study. JEØN removed the geophysical signal from the sea-level
877 measured by the tide gauges. FM wrote the code to analyse the data. All authors contributed to the analysis of
878 the results, and to the writing and the editing of the paper.

879

880 **Competing interests**

881 The authors declare that they have no conflict of interest.

882

883 **Acknowledgements**

884 We would like to thank the two reviewers who significantly helped improved this manuscript. All products are
885 computed based on altimetry missions operated by NASA/CNES (Jason-1), ESA (Envisat, Cryosat-2),
886 CNES/NASA/Eumetsat/NOAA (Jason-2, Jason-3), ISRO/CNES (SARAL). The original data sets are disseminated by
887 AVISO, ESA, NOAA, and PODAAC. Michael Hart-Davis (TUM) is kindly acknowledged for providing the EOT11a
888 tidal model data, and Kristian Breili (Norwegian Mapping Authority) for providing the GIA data. Léon Chafik
889 acknowledges support from the Swedish National Space Agency (Dnr: 133/17, 204/19).

890

891

892

893

894 **References**

895 Abulaitijiang, A., Andersen, O. B., and Stenseng, L.: Coastal sea level from inland CryoSat-2 interferometric SAR
896 altimetry, *Geophys. Res. Lett.*, 42, 1841-1847, <https://doi.org/10.1002/2015GL063131>, 2015.

897

898 Bartlett, M. S.: Some Aspects of the Time-Correlation Problem in Regard to Tests of Significance, *J. R. Stat. Soc.*,
899 98, 536-543, <https://doi.org/10.2307/2342284>, 1935.

900

901 Benveniste, J., Birol, F., Calafat, F., Cazenave, A., Dieng, H., Gouzenes, Y., Legeais, J. F., Léger, F., Niño, F.,
902 Passaro, M., Schwatke, C., and Shaw, A.: Coastal sea level anomalies and associated trends from Jason satellite
903 altimetry over 2002-2018, *Sci. Data*, 7, 1–17, <https://doi.org/10.1038/s41597-020-00694-w>, 2020.

904

905 Bonaduce, A., Pinardi, N., Oddo, P., Spada, G., and Larnicol, G.: Sea-level variability in the Mediterranean Sea
906 from altimetry and tide gauges, *Clim. Dyn.*, 47, 2851-2866, <https://doi.org/10.1007/s00382-016-3001-2>, 2016.

907

908 Breili, K., Simpson, M. J. R., and Nilsen, J. E. Ø.: Observed sea-level changes along the Norwegian coast, *J. Mar.*
909 *Sci. Eng.*, 5, 1-19, <https://doi.org/10.3390/jmse5030029>, 2017.

910
911 Carrère, L. and Lyard, F.: Modeling the barotropic response of the global ocean to atmospheric wind and
912 pressure forcing - Comparisons with observations, *Geophys. Res. Lett.*, 30,
913 <https://doi.org/10.1029/2002GL016473>, 2003.
914
915 Cazenave, A., Palanisamy, H., and Ablain, M.: Contemporary sea level changes from satellite altimetry: What
916 have we learned? What are the new challenges?, *Adv. Space Res.*, 62, 1639-1653,
917 <https://doi.org/10.1016/j.asr.2018.07.017>, 2018.
918
919 Chafik, L., Nilsson, J., Skagseth, and Lundberg, P.: On the flow of Atlantic water and temperature anomalies in
920 the Nordic Seas toward the Arctic Ocean, *J. Geophys. Res. Oceans*, 120, 7897-7918,
921 <https://doi.org/10.1002/2015JC011012>, 2015.
922
923 Chafik, L., Nilsen, J. E. Ø., and Dangendorf, S.: Impact of North Atlantic teleconnection patterns on northern
924 European sea level, *J. Mar. Sci. Eng.*, 5, 1-23, <https://doi.org/10.3390/jmse5030043>, 2017.
925
926 Chafik, L., Nilsen, J. E. Ø., Dangendorf, S., Reverdin, G., and Frederikse, T.: North Atlantic Ocean Circulation and
927 Decadal Sea Level Change During the Altimetry Era, *Sci. Rep.*, 9, 1-9, [https://doi.org/10.1038/s41598-018-](https://doi.org/10.1038/s41598-018-37603-6)
928 [37603-6](https://doi.org/10.1038/s41598-018-37603-6), 2019.
929
930 Cipollini, P., Benveniste, J., Bouffard, J., Emery, W., Fenoglio-Marc, L., Gommenginger, C., Griffin, D., Høyer, J.,
931 Kuparov, A., Madsen, K., Mercier, F., Miller, L., Pascual, A., Ravichandran, M., Shillington, F., Snaith, H., Sturb, P.
932 T., Vandemark, D., Vignudelli, S., Wilkin, J., Woodworth, P., and Zavala-Garay, J.: The Role of Altimetry in Coastal
933 Observing Systems. In: Hall J, Harrison DE, Stammer D (eds) *Proceedings of OceanObs'09: sustained ocean*
934 *observations and information for society*, vol 2. European Space Agency, WPP-306, pp 181–191. (19) (PDF)
935 *Coastal gravity field refinement by combining airborne and ground-based data*.
936 <https://doi.org/10.5270/oceanobs09.cwp.16>, 2010.
937
938 Cipollini, P., Benveniste, J., Birol, F., Joana Fernandes, M., Obligis, E., Passaro, M., Ted Strub, P., Valladeau, G.,
939 Vignudelli, S., and Wilkin, J.: Satellite altimetry in coastal regions, in: *Satellite Altimetry Over Oceans and Land*
940 *Surfaces*, *Surv. Geophys.*, 38, 33-57, <https://doi.org/10.1201/9781315151779>, 2017.
941
942 Frederikse, T., Jevrejeva, S., Riva, R. E. M., and Dangendorf, S.: A consistent sea-level reconstruction and its
943 budget on basin and global scales over 1958-2014, *J. Clim.*, 31, 1267-1280, [https://doi.org/10.1175/JCLI-D-17-](https://doi.org/10.1175/JCLI-D-17-0502.1)
944 [0502.1](https://doi.org/10.1175/JCLI-D-17-0502.1), 2018.
945
946 Frederikse, T., Landerer, F., Caron, L., Adhikari, S., Parkes, D., Humphrey, V. W., Dangendorf, S., Hogarth, P.,
947 Zanna, L., Cheng, L., and Wu, Y. H.: The causes of sea-level rise since 1900, *Nature*, 584, 393-397,
948 <https://doi.org/10.1038/s41586-020-2591-3>, 2020.
949
950 Gill, A. E. and Niller, P. P.: The theory of the seasonal variability in the ocean, *Deep Sea Res. Oceanogr. Abstr.*,
951 20, 141-177, [https://doi.org/10.1016/0011-7471\(73\)90049-1](https://doi.org/10.1016/0011-7471(73)90049-1), 1973.
952

953 Gómez-Enri, J., Vignudelli, S., Quartly, G. D., Gommenginger, C. P., Cipollini, P., Challenor, P. G., and Benveniste,
954 J.: Modeling Envisat RA-2 waveforms in the coastal zone: Case study of calm water contamination, *IEEE Geosci.*
955 *Remote Sensing Lett.*, 7, 474–478, <https://doi.org/10.1109/LGRS.2009.2039193>, 2010.

956

957 Hermans, T. H. J., Gregory, J. M., Palmer, M. D., Ringer, M. A., Katsman, C. A., and Slangen, A. B. A.: Projecting
958 Global Mean Sea-Level Change Using CMIP6 Models, *Geophys. Res. Lett.*, 48,
959 <https://doi.org/10.1029/2020GL092064>, 2021.

960

961 Ji, M., Reynolds, R. W., and Behringer, D. W.: Use of TOPEX/Poseidon sea level data for Ocean analyses and
962 ENSO prediction: Some early results, *J. Clim.*, 13, 216-231, [https://doi.org/10.1175/1520-](https://doi.org/10.1175/1520-0442(2000)013<0216:UOTPSL>2.0.CO;2)
963 [0442\(2000\)013<0216:UOTPSL>2.0.CO;2](https://doi.org/10.1175/1520-0442(2000)013<0216:UOTPSL>2.0.CO;2), 2000.

964

965 Lichter, M., Vafeidis, A. T., Nicholls, R. J., and Kaiser, G.: Exploring data-related uncertainties in analyses of land
966 area and population in the “Low-Elevation Coastal Zone” (LECZ), *J. Coast. Res.*, 27 (4), 757-768,
967 <https://doi.org/10.2112/JCOASTRES-D-10-00072.1>, 2011.

968

969 Liebmann, B., Dole, R. M., Jones, C., Bladé, I., and Allured, D.: Influence of choice of time period on global
970 surface temperature trend estimates, *Bull. Am. Meteorol. Soc.*, 91, 1485-1491,
971 <https://doi.org/10.1175/2010BAMS3030.1>, 2010.

972

973 Madsen, K. S., Høyer, J. L., Suursaar, Ü., She, J., and Knudsen, P.: Sea Level Trends and Variability of the Baltic
974 Sea From 2D Statistical Reconstruction and Altimetry, *Front. Earth Sci.*, 7,
975 <https://doi.org/10.3389/feart.2019.00243>, 2019.

976

977 Nerem, R. S., Chambers, D. P., Choe, C., and Mitchum, G. T.: Estimating Mean Sea Level Change from the TOPEX
978 and Jason Altimeter Missions, *Mar. Geod.*, 33, 435-446, <https://doi.org/10.1080/01490419.2010.491031>, 2010.

979

980 Nicholls, R. J.: Planning for the Impacts of Sea Level Rise, *Oceanography*, 24, 144–157, 2011.

981 Oelsmann, J., Passaro, M., Dettmering, D., Schwatke, C., Sanchez, L., and Seitz, F.: The Zone of Influence:
982 Matching sea level variability from coastal altimetry and tide gauges for vertical land motion estimation, *Ocean*
983 *Sci.*, 17, 35-57, <https://doi.org/10.5194/os-2020-29>, 2021.

984

985 Passaro, M., Cipollini, P., Vignudelli, S., Quartly, G. D., and Snaith, H. M.: ALES: A multi-mission adaptive
986 subwaveform retracker for coastal and open ocean altimetry, *Remote Sens. Environ.*, 145, 173-189,
987 <https://doi.org/10.1016/j.rse.2014.02.008>, 2014.

988

989 Passaro, M., Cipollini, P., and Benveniste, J.: Annual sea level variability of the coastal ocean: The Baltic Sea-
990 North Sea transition zone, *J. Geophys. Res. Oceans*, 120, 3061-3078, <https://doi.org/10.1002/2014JC010510>,
991 2015.

992

993 Passaro, M., Dinardo, S., Quartly, G. D., Snaith, H. M., Benveniste, J., Cipollini, P., and Lucas, B.: Cross-calibrating
994 ALES Envisat and CryoSat-2 Delay-Doppler: A coastal altimetry study in the Indonesian Seas, *Adv. Space Res.*, 58,
995 289-303, <https://doi.org/10.1016/j.asr.2016.04.011>, 2016.

996
997 Passaro, M., Smith, W., Schwatke, C., Piccioni, G., Dettmering, D.: Validation of a global dataset based on
998 subwaveform retracking: improving the precision of pulse-limited satellite altimetry. OSTST Meeting 2017, Miami,
999 USA, 2017.
1000
1001 Passaro, M., Rose, S. K., Andersen, O. B., Boergens, E., Calafat, F. M., Dettmering, D., and Benveniste, J.: ALES+:
1002 Adapting a homogenous ocean retracker for satellite altimetry to sea ice leads, coastal and inland waters,
1003 Remote Sens. Environ., 211, 456-471, <https://doi.org/10.1016/j.rse.2018.02.074>, 2018.
1004
1005 Passaro, M., Müller, F. L., Oelmann, J., Rautiainen, L., Dettmering, D., Hart-Davis, M. G., Abulaitijiang, A.,
1006 Andersen, O. B., Høyer, J. L., Madsen, K. S., Ringgaard, I. M., Särkkä, J., Scarrott, R., Schwatke, C., Seitz, F.,
1007 Tuomi, L., Restano, M., and Benveniste, J.: Absolute Baltic Sea Level Trends in the Satellite Altimetry Era: A
1008 Revisit, Front. Mar. Sci., 8, <https://doi.org/10.3389/fmars.2021.647607>, 2021.
1009
1010 Picaut, J., Hackert, E., Busalacchi, A. J., Murtugudde, R., and Lagerloef, G. S. E.: Mechanisms of the 1997–1998 El
1011 Niño–La Niña, as inferred from space-based observations, J. Geophys. Res., 107,
1012 <https://doi.org/10.1029/2001jc000850>, 2002.
1013
1014 Raj, R. P., Andersen, O. B., Johannessen, J. A., Gutknecht, B. D., Chatterjee, S., Rose, S. K., Bonaduce, A.,
1015 Horwath, M., Ranndal, H., Richter, K., Palanisamy, H., Ludwigsen, C. A., Bertino, L., Nilsen, J. E. Ø., Knudsen, P.,
1016 Hogg, A., Cazenave, A., and Benveniste, J.: Arctic sea level budget assessment during the grace/argo time
1017 period, Remote Sens., 12, <https://doi.org/10.3390/rs12172837>, 2020.
1018
1019 Richter, K., Nilsen, J. E. Ø., and Drange, H.: Contributions to sea level variability along the Norwegian coast for
1020 1960-2010, J. Geophys. Res., 117, <https://doi.org/10.1029/2011JC007826>, 2012.
1021
1022 Richter, K., Meyssignac, B., Slangen, A. B. A., Melet, A., Church, J. A., Fettweis, X., Marzeion, B., Agosta, C.,
1023 Ligtenberg, S. R. M., Spada, G., Palmer, M. D., Roberts, C. D., and Champollion, N.: Detecting a forced signal in
1024 satellite-era sea-level change, Environ. Res. Lett., 15, <https://doi.org/10.1088/1748-9326/ab986e>, 2020.
1025
1026 Rose, S. K., Andersen, O. B., Passaro, M., Ludwigsen, C. A., and Schwatke, C.: Arctic ocean sea level record from
1027 the complete radar altimetry era: 1991-2018, Remote Sens., 11, <https://doi.org/10.3390/rs11141672>, 2019.
1028
1029 Siegmund, F., Johannessen, J., Drange, H., Mork, K. A., and Korabely, A.: Steric height variability in the Nordic
1030 Seas, J. Geophys. Res., 112, <https://doi.org/10.1029/2007JC004221>, 2007.
1031
1032 Simpson, M. J. R., Nilsen, J. E. Ø., Ravndal, O. R., Breili, K., Sande, H., Kierulf, H. P., Steffen, H., Jansen, E., Carson,
1033 M., and Vestøl, O.: Sea Level Change for Norway Past and Present Observations and Projections to 2100, Tech.
1034 rep., Norwegian Centre for Climate Services report 1/2015. ISSN 2387–3025, 156 pp., 2015.

1035

1036 Simpson, M. J. R., Ravndal, O. R., Sande, H., Nilsen, J. E. Ø., Kierulf, H. P., Vestøl, O., and Steffen, H.: Projected
1037 21st century sea-level changes, observed sea level extremes, and sea level allowances for Norway, *J. Mar. Sci.*
1038 *Eng.*, 5, <https://doi.org/10.3390/jmse5030036>, 2017.

1039

1040 Stammer, D., Cazenave, A., Ponte, R. M., and Tamisiea, M. E.: Causes for contemporary regional sea level
1041 changes, *Annu. Rev. Mar. Sci.*, 5, 21-46, <https://doi.org/10.1146/annurev-marine-121211-172406>, 2013.

1042

1043 Volkov, D. L. and Pujol, M. I.: Quality assessment of a satellite altimetry data product in the Nordic, Barents, and
1044 Kara seas, *J. Geophys. Res.*, 117, <https://doi.org/10.1029/2011JC007557>, 2012.

1045

1046 Wackernagel, H.: *Multivariate Geostatistics*, 3rd ed., Springer, Berlin, Heidelberg, 1–388 pp., 2003.

1047

1048 Woodworth, P. L.: A note on the nodal tide in sea level records, *J. Coastal Res.*, 28 (2), 316-323,
1049 <https://doi.org/10.2112/JCOASTRES-D-11A-00023.1>, 2012.

1050

1051 Xu, X.-Y., Xu, K., Xu, Y., and Shi, L.-W.: Coastal Altimetry: A Promising Technology for the Coastal Oceanography
1052 Community, in: *Estuaries and Coastal Zones - Dynamics and Response to Environmental Changes*, *Surv.*
1053 *Geophys.*, 40, 1351-1397, <https://doi.org/10.5772/intechopen.89373>, 2019.

1054

1055 Zhang, Z., Lu, Y., and Hsu, H.: Detecting ocean currents from satellite altimetry, satellite gravity and ocean data,
1056 in *Dynamic Planet*, *International Association of Geodesy Symposia*, edited by P. Tregoning, and C. Rizos,
1057 Springer, Berlin.
1058 https://doi.org/10.1007/978-3-540-49350-1_3, 2007.

1059

1060

1061

1062